THERMAL ANALYSIS OF EUTECTIC MODIFIED AND GRAIN REFINED ALUMINUM-SILICON ALLOYS

A THESIS SUBMITTED TO
THE GRADUATE SCHOOL OF NATURAL AND APPLIED SCIENCES
OF
MIDDLE EAST TECHNICAL UNIVERSITY

BY

H.EROL İSLAMOĞLU

IN PARTIAL FULFILLMENT OF THE REQUIREMENTS
FOR
THE DEGREE OF MASTER OF SCIENCE
IN
METALLURGICAL AND MATERIALS ENGINEERING

SEPTEMBER 2005

Approval of the Graduate School of Natural and Applied Sciences

_____

Prof. Dr. Canan Özgen
Director

I certify that this thesis satisfies all the requirements as a thesis for the degree of Master of Science.

_____

Prof. Dr. Tayfur Öztürk
Head of Department

This is to certify that we have read this thesis and that in our opinion it is fully adequate, in scope and quality, as a thesis for the degree of Master of Science.

_____

Prof. Dr. Ali Kalkanlı
Supervisor

Examining Committee Members

Prof. Dr. Ahmet Geveci (METU,METE) _____

Prof. Dr. Ali Kalkanlı (METU,METE) _____

Prof.Dr. Filiz Sarıoğlu (METU,METE) _____

Assoc.Prof.Dr.Hakan Gür (METU,METE) _____

Prof.Dr. Mustafa I. Gökler (METU,ME) _____

I hereby declare that all information in this document has been obtained and presented in accordance with academic rules and ethical conduct. I also declare that, as required by these rules and conduct, I have fully cited and referenced all material and results that are not original to this work.

Name, Last name : H.EROL İSLAMOĞLU

Signature :

ABSTRACT

THERMAL ANALYSIS OF EUTECTIC MODIFIED AND GRAIN REFINED ALUMINUM-SILICON ALLOYS

İslamoğlu, Hamza Erol

M.Sc., Metallurgical and Materials Engineering Department

Supervisor : Prof. Dr. Ali Kalkanlı

September 2005, 94 pages

A series of $AlSi_9Mg$ alloys were prepared and tested to reveal the effect of addition sequence and timing of grain refiner and eutectic modifier. AlSr10 master alloy was used as an modification reagent, and also for grain refiner AlTi5B master alloy was used. The depression at the eutectic temperature due to the addition of modifier and decrease in the amount of undercooling at the liquidus due to the presence of grain refiner were examined by the cooling curves which were obtained by the Alu-Therm instrument, which is the aluminum thermal analyzer of the Heraeus Electro-Nite.

The alloys that were both modified and grain refined were subsequently poured as tensile test specimen shapes in permanent die casting mould for four times at 60 minutes time intervals, meanwhile thermal analysis of the alloys were also made.

In this work the effect of grain refinement and modification agent, also the determination of the optimum time to pour after adding these agents were studied by aluminum thermal analyzer. The parameters obtained from this

analyzer are compared with the microstructures; to see the effect of these agents on mechanical properties, hardness, tensile strength and percent elongation values were investigated.

In this study the possibility of predicting the mechanical properties prior to casting by thermal analysis method was examined by regression analysis method. By this method relationship between thermal analysis parameters and mechanical properties was established.

Keywords: Grain refinement, eutectic modification, thermal analysis of aluminum alloys, cooling curve.

öz

ÖTEKTİK MODİFİKASYONU VE TANE İNCELTMESİ YAPILMIŞ ALÜMİNYUM-SİLİKON ALAŞIMLARININ TERMAL ANALİZİ

İslamoğlu, Hamza Erol
Yüksek Lisans, Metalurji ve Malzeme Mühendisliği Bölümü
Tez Yöneticisi : Prof. Dr. Ali Kalkanlı

Eylül 2005, 94 Sayfa

Tane inceltici ve ötektik modifiye edicilerin eklenme sırası ve eklenmesinden sonraki bekleme süresinin etkisini gözlemlemek amacı ile dokuz AlSi9Mg alaşımı hazırlanmıştır. Modifiye edici olarak Sr, AlSr10 alaşımı şeklinde, tane inceltici olarak da AlTi5B alaşımı kullanılmıştır. Sıvı metale eklenen modifiye edici ve tane incelticinin etkisi olarak ötektik sıcaklığındaki düşüşler ve sıvılaşma sıcaklığında oluşan aşırı soğuma miktarlarındaki azalmalar, Heraeus Electro-Nite marka Alu-Therm model alüminyum thermal analiz sistemi ile elde edilen soğuma eğrileri ile incelenmiştir.

Tane inceltmesi ve ötektik modifikasyonu yapılmış dokuz farklı kompozisyondaki alaşımdan çekme deneyi numunesini elde etmek amacı ile alaşımlar 15 dakika ara ile 4 seferde metal kalıplara dökülmüştür ve aynı anda termal analizleri de yapılmıştır.

Bu çalışmada tane inceltici olarak kullanılan AlTi5B ve modifiye edici olarak kullanılan AlSr10 bileşiklerinin etkisi ve bu bileşiklerin eklenmesinden sonra

döküm için en uygun sürenin bulunması için termal analiz yöntemi kullanılmıştır. Bu doğrultuda Heraeus Electro-Nite üretimi olan Alu-Therm termal analiz sisteminin soğuma eğrilerinden hesaplamış olduğu parametreler ait olduğu dökümün içyapısı ile karşılaştırılmıştır. Ayrıca etkileri daha iyi görmek amacı ile dökümlerin mekanik özelliklerinden sertlik, çekme mukavemeti ve yüzde uzamaları incelenmiştir.

Çalışmada ayrıca döküm parçasının mekanik özelliklerini daha dökülmeden önce termal analiz yöntemi ile tahmin edebilme olasılığı göz önüne alınarak, termal analiz parametreleri ile mekanik test sonuçları arasındaki bağlantıların regresyon denklemleri ile bulunması üzerine de çalışılmıştır.

Anahtar Kelimeler: Tane inceltme, ötektik modifikasyon, alümiyum alaşımlarının termal analizi, soğuma eğrisi.

To My Mom, Dad
and
my sister Sezin

ACKNOWLEDGMENTS

I am grateful to Prof.Dr.Ali Kalkanlı for his guidance and insightful comments and helpful advices which always encouraged me to work harder with trust and enthusiasm.

I wish to express my gratitude to the General Manager of the Heraeus Electro-Nite Turkey, Haluk Güldür, who gave his approval to this project and supported it during the years it took to bring it to fruition.

I also want to thank my sister for her encouragement with insightful and valuable comments.

Finally I want to thank to my family for their invaluable spiritual support, special care and faith in me. In every stage of my life, they have been just beside me with their endless love, patience and encouragement.

TABLE OF CONTENTS

APPENDICES

LIST OF TABLES

TABLE

LIST OF FIGURES

CHAPTER 1

INTRODUCTION

Cast aluminum alloys have a wide range of applications in manufacturing industry especially automotive and aerospace. When alloyed with silicon, good castability, resistance to hot tearing, reasonable mechanical properties and excellent corrosion resistance may be achieved. In addition, since silicon increases in volume during solidification, the susceptibility of castings to shrinkage defects is reduced. The silicon phase can also form with different morphologies, e.g. rod, flake, fiber, and therefore depending upon solidification conditions and impurity elements such as sodium, strontium or phosphorus, a range of properties can in theory be achieved from a specific alloy composition (Nafisi (2004)).

To improve the mechanical properties of the aluminum casting, refining and modifying the microstructure is one of the most widely used technique. A fine equiaxed grain size in the castings leads to many benefits, such as improved feeding characteristics, uniformed distribution of second phases and microporosity and uniformity of properties and machinability (Johnsson (1992)).

Al-Ti or Al-Ti-B master alloys are added to obtain fine grain size. Also for modification of the structure Na or Sr is added to melt. Unmodified Al-Si alloys contain large flakes of Si crystals. This unmodified Si structure is brittle and harmful to the mechanical properties of the castings. It creates localized stress concentrations and planes of weakness that enhance

crack propagation in castings. Such castings exhibit poor ductility and brittle fracture properties. Therefore, the successful use of aluminum alloys depends on the modification of Si structures from large flakes into finer structures (Jiang (1990)).

In industry controlling the refining of the grain size and modification of the structure have great importance to save time and money. The best and the fastest technique to control these parameters is thermal analysis of the melt before pouring the casting. Thermal analysis is a process control technique by which grain refinement and modification treatment are monitored. The method is based on recording and evaluating the cooling curve of a solidifying sample. By the help of the undercooling on the liquidus of the cooling curve of an aluminum alloy obtained by thermal analysis the nucleation potential of the alloy and also the grain size of the structure can be understood. If little or no undercooling is present on the liquidus, it corresponds to high number of nucleation sites so fine grain size will be achieved. On the other hand if important undercooling is present on the liquidus, it corresponds to less nucleation sites, so larger grain size will be obtained. Also by the help of thermal analysis, the nucleation potential of the melt can be checked. Because of the action of nucleation agents (Na and Sr) the eutectic silicon particles nucleate at a lower temperature. Thus modification lowers the eutectic temperature (Te), the higher the modification potential the lower eutectic temperature (Te). Therefore by knowing the exact eutectic temperature of the unmodified alloy, the necessary modification can be calculated by comparing the unmodified alloy's eutectic temperature to that of the modified one.

In this study, the cooling curves and their first derivatives for nine different Aluminum-Silicon alloys were prepared by changing the Ti percentage from 0.04% to 0.15% and Sr percentage from 0.013% to 0.017%. The aim of preparing these nine alloys was to find the optimum amount of Ti and Sr to obtain fine grain size and good modification. And these nine alloys were

examined by Alu-Therm instrument, which is the aluminum thermal analyzer of Heraeus Electro-Nite. The metallographic examination, tensile strength results and hardness values of these nine different alloys were collected to investigate the relationship between the parameters that Alu-Therm thermal analyzer gave. To investigate the relation, regression analysis technique was used.

In addition, to find the optimum contact time for the grain refinement, alloys were examined by the parameters of the Alu-Therm thermal analyzer, and these parameters were compared with the metallographic examination results. Also to find the best sequence for alloy preparation different procedures were tried.

CHAPTER 2

THEORY

2.1 Aluminum Casting Alloys

Aluminum casting alloys are the most versatile of all common foundry alloys and generally have the highest castability ratings. As casting materials, aluminum alloys have the following favorable characteristics:

i) Good fluidity for filling thin sections
ii) Low melting point relative to those required for many other metals
iii) Rapid heat transfer from the molten aluminum to the mold, providing shorter casting cycles
iv) Hydrogen is the only gas with appreciable solubility in aluminum and its alloys, and hydrogen solubility in aluminum can be readily controlled by processing methods.
v) Many aluminum alloys are relatively free from hot-short cracking and tearing tendencies.
vi) Chemical stability
vii) Good as-cast surface finish with lustrous surfaces and little or no blemishes (Davis (1994)).

2.1.1 Aluminum-Silicon Alloys

Aluminum-silicon castings constitute 85% to 90% of the total aluminum cast parts produced. Aluminum alloys containing silicon as the major alloying element offer excellent castability, good corrosion resistance, and can be machined and welded (Gruzleski (1999)).

Strengthening of Al-Si alloys is achieved by adding small amounts of Cu, Mg or Ni. In this family of alloys of hypoeutectic composition, silicon provides good casting properties and copper improves tensile strength, machinability and thermal conductivity at the expense of a reduction in ductility and corrosion resistance (Gruzleski (1999)).

2.2 Grain Structure Control

Reduction in grain size is brought about by the efficient heterogeneous nucleation of the α-aluminum phase. This can be achieved through crystal multiplication using mechanical or fluid flow forces to detach dendrite arms, but in practice chemical additives are used to provide the necessary nuclei (Davis (1994)).

Other factors that affect the ultimate cast grain size are alloy composition, freezing rate, temperature gradient in the melt, and casting method. The commercially available chemical additives usually provided in the form of aluminum-base master alloy compositions and casting conditions are used in practice (Davis (1994)).

2.3 Grain Refining of Aluminum-Silicon Foundry Alloys

There are three principal methods for achieving grain refinement in aluminum-silicon alloys:

i) rapid cooling,
ii) mechanical agitation of the melt by manual or electromagnetic stirring, or ultrasonic vibration during solidification,
iii) addition of a grain refining salt or a master alloy to the melt (Chemical grain refinement).

In the first method, a fine grain structure is formed in the casting due to curtailment of grain growth during the solidification process. In the second method, grain refinement is accomplished by mechanically breaking up newly formed dendrites in the semi-solid state (Gruzleski (1999)).

Normally the degree of refinement is dependent on the energy input into the solidifying metal. Although workable in some situations, both methods are generally uneconomical or impractical in a production environment (Gruzleski (1999)).

By far the most widely used procedure in the industry is the addition of a specific nucleating agent in the form of a master alloy or salt. The use of a master alloy is the preferred choice in most foundries as it is convenient and does not have the problems often associated with a salt addition such as fuming, reactivity with elements in the melt and unpredictable recovery rate(Gruzleski (1999)).

2.3.1 Chemical Grain Refinement

This is the most widely practiced and most foolproof method of grain refinement. In chemical grain refinement, additions of effective nuclei are made to the melt through either master alloys or fluxes. A fine grain size is promoted by the presence of an enhanced number of nuclei, and solidification proceeds at very small undercooling (Gruzleski (1999)).

The chemical grain refinement of aluminum and its alloys has been practiced for over 50 years, mostly by primary aluminum producers in ingot casting. The foundry industry has more or less borrowed the techniques developed by primary producers, but as we shall see, there is evidence to indicate that the best grain refiners for wrought alloys are not necessarily the best for casting alloys (Gruzleski (1999)).

2.3.1.1 Titanium and Titanium-Boron Grain Refinement

Aluminum alloys are grain refined by the addition of typically from 0.02 to 0,15 % Ti or Ti-B mixtures in the range of 0.01 – 0.03% Ti and 0.01% B. The titanium and boron are added via master alloys available in ingot or waffle form or as salt mixtures. Grain refinement by the addition of Ti alone is reasonably well understood; however, the role of boron which acts to make the titanium refinement more effective is still the subject of great controversy (Gruzleski (1999)).

It is well known that the processing conditions of Al-Ti-B master alloys affect the final performance and that not all master alloys are created equally. Grain refining ability seems to depend on the morphology of the intermetallic phases which are present in the alloy. Poor grain refiners contain blocky type $TiAl_3$ crystals, which are similar to those found in binary

Al-Ti grain refiners. Here the boron has apparently exerted no influence on the intermetallic phase during manufacture of the grain refiner. Good grain refiners contain duplex intermetallic phases which consist of $TiAl_3$ particles whose surface is covered with small boride particles, perhaps TiB_2 or $(Ti,Al)B_2$ (Gruzleski (1999)).

The conditions favoring the formation of the duplex particles in the master alloy are quite specific and are related to the holding time in the liquid state after the master alloy has been manufactured, but before it is cast (Gruzleski (1999)).

Primary alloys contain little silicon (less than 0.05 %), and in these alloys, titanium or titanium-boron mixtures provide powerful grain refinement. Boron, by itself, will not grain refine at all. In foundry alloys, the picture is quite different, since silicon, copper and zinc actually hinder titanium grain refinement. Surprisingly, boron acting on its own is a much better grain refiner. The discovery of this important difference in grain refining behavior between wrought and cast alloys underscores once again the importance of melt chemistry and the need for research and development on casting alloys (Gruzleski (1999)).

Recently, an improved grain refiner for cast alloys has been put on the market. It contains 2.5% Ti and 2.5% B. Although high-boron grain refiners appear to offer many advantages to the aluminum foundry industry, one of their negative aspects appears to be a tendency to contribute to hard spots in castings. This effect is not well documented at present (Gruzleski (1999)).

2.3.1.2 Aluminum-Titanium-Carbon Grain Refinement

A commercial master alloy based on the Al-Ti-C system was introduced by Anglo-Blackwells in 1986. The alloy had a nominal composition of Al-6%Ti-0.02%C and was used successfully to control the as-cast grain structure in Properzi cast 1350 alloy,continuously cast plate and ingot used to produce sheet for a brightened and anodized application (Granger (1992)). The principal drawback to this alloy composition was the high ratio of Ti:C, which results in high titanium additions to provide enough TiC nuclei to control grain structure. This gave impetus to request further developmental work which was undertaken by Shieldalloy Metallurgical Corporation (SMC) starting in 1993. The goal of this activity was to manufacture an Al-Ti-C grain refining alloy that would have a substantially reduced Ti:C ratio in addition to the otherdesirable characteristics such as a small TiC particle size, low level of nonmetallic inclusions, absence of unreacted titanium, no aluminum carbides, and would provide consistent grain refining performance in a wide selection of aluminum alloys produced under a range of casting conditions (Whitehead (1997)).

2.3.2 Nucleation mechanism of Grain Refinement

The nucleant effects i.e. which particle and its characteristics nucleate α-aluminum, has been the subject of intensive research. Lately the solute effect i.e. the effect of dissolved titanium on grain refinement has come into forefront of grain refinement research (Kashyap (2001)). And the solute effects on the grain refinement are detailed here.

Grain refinement can be understood to be directly related to the nucleation and growth process of aluminum grains. This is based on the nucleation ideas of Volmer and Weber (1925). The theory involves homogeneous and heterogeneous nucleation. In a pure metal solidifying, the critical nucleus size for survival is given by

$$r^*_{\text{hom}\,ogeneous} = \frac{-2\gamma_{sL}}{\Delta G_v} \qquad (1)$$

The free energy barrier is given by

$$\Delta G^*_{\text{hom}\,ogeneous} = \frac{16\pi\gamma^3_{sL}}{3\Delta G^2_V} \qquad (2)$$

where, γ_{sL} is the interface surface energy of a solid–liquid interface in J/m^2; assuming the specific heats of liquid and solid are similar, ΔG_v is the driving force for solidification

$$\cong \Delta T\Delta S = \frac{\Delta H_f \Delta T}{T_m}$$

ΔT is the undercooling below the liquidus temperature *K*, ΔS the entropy change for liquid to solid phase transformation,J/K/m^3 , ΔH_f the enthalpy of solidification and T_m the melting temperature. If the embryo of the solid is greater than critical radius, $r^*_{\text{homogeneous}}$, the embryo will survive and become a nucleus.

In heterogeneous nucleation, the critical nucleus size is

$$r^*_{heterogeneous} = \frac{-2\gamma_{sL}}{\Delta G_v} \qquad (3)$$

(1) and (3) are identical for both homogeneous and heterogeneous nucleation and the free energy barrier is

$$\Delta G^{*}_{heterogeneous} = \frac{16\pi\gamma_{sL}^{3}}{3\Delta G_{v}^{2}} f(\theta) \qquad (4)$$

Where $f(\theta)$ is a function of the contact angle θ on the substrate on which nucleation takes place. Figure 1 shows the solid nucleating on a substrate in a liquid. Figure 2 shows the variation of $f(\theta)$ with θ and since $f(\theta)$ is always ≤ 1, the critical free energy for heterogeneous nucleation is always less than or equal to that for homogeneous nucleation. However, it is clear that potential heterogeneous substrates are those with θ close to zero.

The values of undercooling, ΔT is of the order 1–2 K for observable nucleation rates in commercial aluminium alloys with grain refiners. Therefore, clearly heterogeneous nucleation is taking place. The following simplified expression for heterogeneous nucleation rate per unit volume in $m^{-3}\ s^{-1}$ is

$$I^{v}_{heterogeneous} = 10^{18} N_{v}^{p} \exp\left[\frac{-16\pi\gamma_{sL}^{3} f(\theta)}{3K_{B}\Delta S^{2}\Delta T^{2}}\right] \qquad (5)$$

where, K_B is the Boltzman's constant, J/K, N_v^p the number of nuclei/m^3 , and $I^{v}_{heterogeneous}$ the heterogeneous nucleation rate # of nuclei/m^3.sec (McCartney (1989)).

Therefore, it can be seen that if contact angle is close to zero, wetting of the substrate for nucleation is promoted and nucleation rate increases (McCartney (1989)).

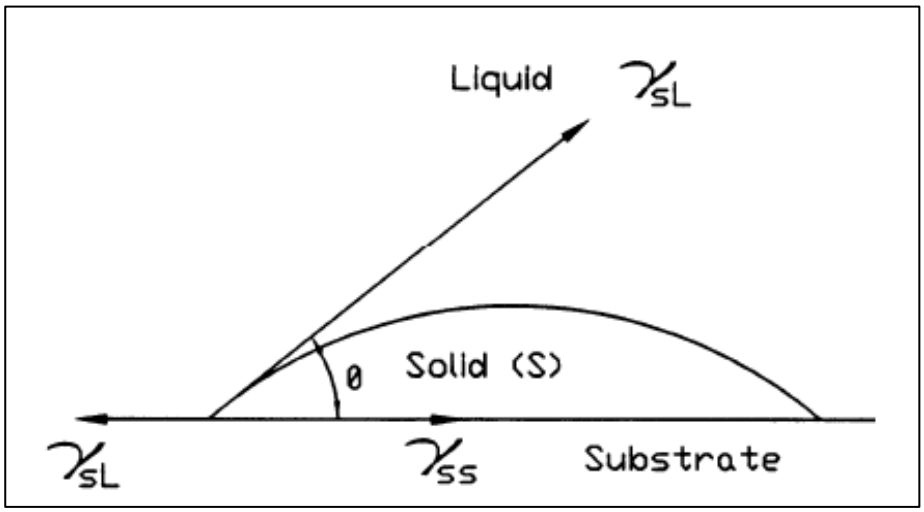

Figure 1. Schematic representation showing the formation of spherical cap of solid(s) on a substrate, contact angle and surface tension forces

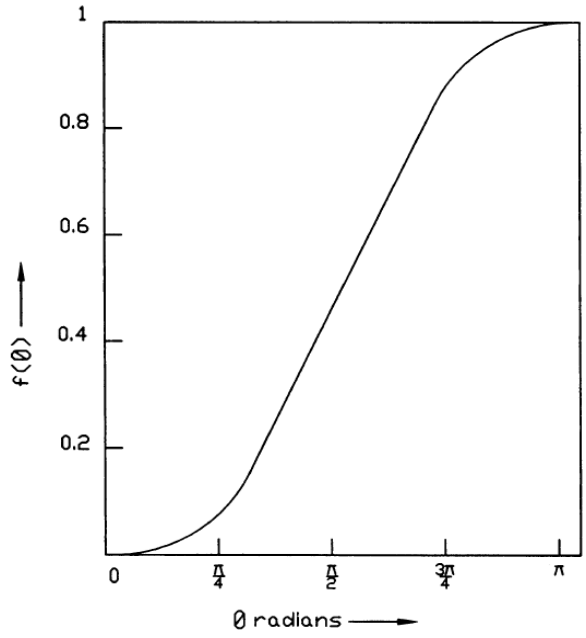

Figure 2. Showing the variation of $f(\theta)$ with θ where $f(\theta)$ is equal to $(2 - 3\cos\theta + \cos^3\theta)/4$

2.3.3 Growth of Nuclei

Once nucleation takes place, more importantly heterogeneous nucleation, the growth front of the nuclei is seldom planar. The well known constitutional supercooling occurs as solute is rejected at the interface and the criterion is given by (Kurz and Fisher 1984).

$$\frac{G_L}{R} \geq \frac{-m_L C_o (1-k)}{kD_L} \qquad (6)$$

where, G_L is the temperature gradient in the liquid ahead of the solid–liquid interface (K/m), R the growth rate of solid liquid interface (m/sec), m_L the liquidus slope of phase diagram (K/wt%), C_0 the bulk alloy composition in the liquid (wt%), k the partition coefficient between solid and liquid, and D_L the diffusion coefficient of the solute in the liquid (m^2/sec).

Normally in a casting we have a columnar zone and a central portion of equiaxed crystals (Flemings (1974a)). The columnar dendrites grow in [1 0 0] directions in the cubic system and growth direction is antiparallel to the heat flow direction. The equiaxed dendrites grow in the same direction of heat flow i.e. radially outward. The formation of equiaxed crystals is due to dendrite arm melt off (Flemings (1974b)) which provides nuclei for equiaxed crystals.

2.3.4 Nucleant effects in grain refinement

Way back in 1940s, Cibula (1949) postulated the carbide/boride theory of grain refinement wherein TiC and/or TiB_2 crystals nucleate solid aluminum by heterogeneous nucleation. Contradicting the above, Crossley and

Mondolfo (1951) proposed the peritectic theory where $TiAl_3$ particles in the master alloy nucleate solid aluminum by a peritectic reaction:

$L+TiAl_3 \rightarrow$ α-aluminum

There has been much debate between these two theories in the literature for the past 50 years (McCartney 1989; Mohanty *et al* 1995; Easton and St. John 1999). Borides are added via the master alloy Al–Ti–B and residual carbon reacts with Ti to form TiC. There is a lot of debate on the stability of TiC in Al melts (Fine and Conley 1990; Rapp and Zheng 1991; Banerji *et al* 1994). Banerji and Reif (1986) have processed Al–Ti–C master alloy for grain refinement of aluminum. The nucleating behavior of all the borides can be discussed concurrently, as TiB_2 and AlB_2 are isomorphous and hexagonal with lattice parameters, *a* = 0.30311 nm and *c* = 0.32291 nm and *a* = 0.3009 nm and *c* = 0.3262 nm, respectively (Arnberg *et al* 1982). The mixed boride phase (Al, Ti)B_2 is formed by replacement of titanium atoms by aluminum atoms in the lattice.

When Al–Ti–B master alloy is added so that titanium is present at hypoperitectic levels (< 0.15 %Ti) as shown in Figure 3, often boride particles or boride agglomerates are found in the centers of grains, with titanium enriched dendrites growing out of them (Johnsson *et al* 1993). This evidence suggests that borides nucleate α-Al. But borides were thought to be poor nucleants or at least not as effective as $TiAl_3$ (Guzowski *et al* 1987).

Mohanty *et al* (1995) have recently confirmed that borides get pushed to the grain boundaries and no grain refinement is observed if no solute titanium is present, which shows that the lattice disregistry between borides and α-aluminum is large indicating that borides act as poor nucleants. It is also observed (Maxwell and Hellawell 1972) that the borides need some undercooling while aluminides need none. In comparison $TiAl_3$ is known to

be a powerful refiner. When present at hyperperitectic concentrations, dramatic grain refinement was observed (Crossley and Mondolfo 1951) and also $TiAl_3$ was found at the centers of grains with multiple orientation relationship (Davies *et al* 1970; Arnberg *et al* 1982) with Al matrix. From this evidence, it can be concluded that $TiAl_3$ is a better refiner than the TiB_2 which is why the phase diagram theories were developed (i.e. by peritectic reaction).

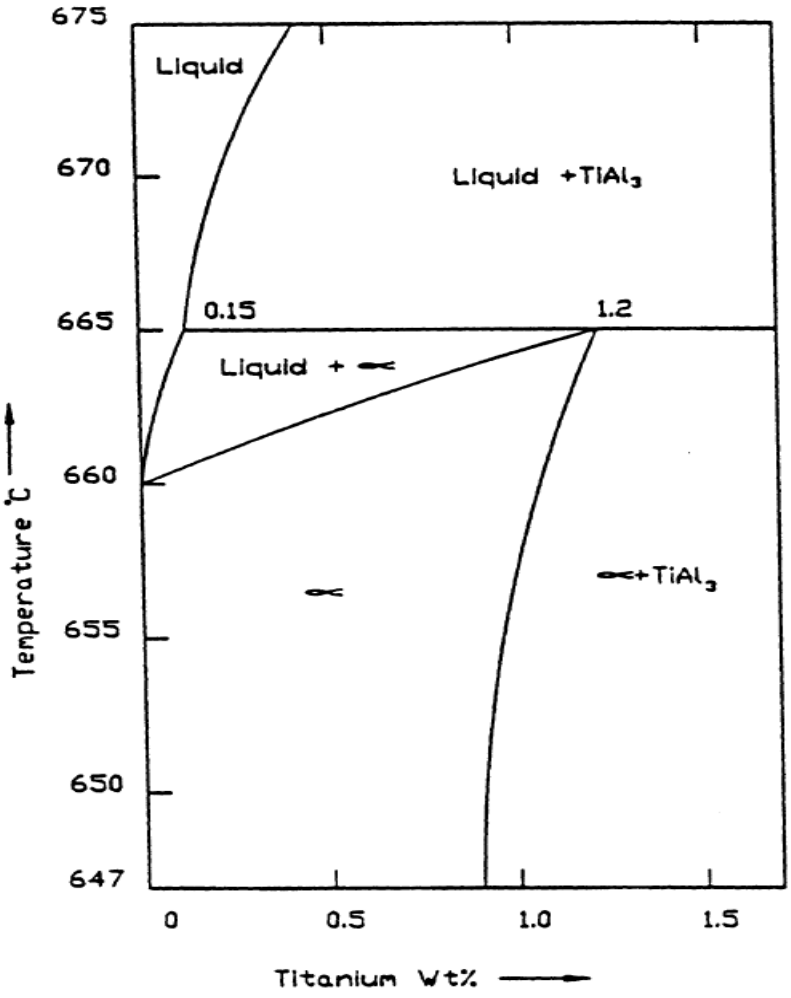

Figure 3. Aluminum end of Al-Ti phase diagram showing 0.15% Ti as the peritectic concentration

2.3.4.1 Phase Diagram Theory

Here in these theories, nucleants particle is taken to be $TiAl_3$. It is suggested that boron addition shifts the peritectic composition (0.15 wt% Ti) to smaller levels which according to Marcantonio and Mondolfo (1971) and Mondolfo *et al* (1987) is 0.05%. This allows $TiAl_3$ to be stable at low titanium levels. Jones and Pearson (1976) and Sigworth (1984, 1986) have performed theoretical thermodynamic calculations and have shown that boron does not alter the Al–Ti phase diagram. Alternatively it has been argued that $TiAl_3$ crystals from the master alloy are stable at low titanium levels in the melt. It has been shown by several researchers, particularly, Guzowski *et al* (1987), that the aluminides take about 30 min to dissolve at 700°C. This leads to the well known effect known as 'fade' where grain size increases with holding time at the pouring temperature. Therefore, at low concentrations of titanium < 0.15 %Ti (peritectic composition), $TiAl_3$ is not stable and will not act as nucleation sites for aluminum.

2.3.4.2 Peritectic Hulk Theory

This theory was very popular in the late 1980s and early 1990s supported by Vader and Noordegraaf (1989) and Backerud *et al* (1991). This theory assumes that $TiAl_3$ is a powerful nucleant than TiB_2. Therefore, it tries to explain how the borides could slow the dissolution rate of $TiAl_3$ when Al–Ti-B master alloy is added to the aluminum melt, so that the more powerful nuclei remain active longer. It suggests that the borides form a shell around the aluminides and hence slow the dissolution of the aluminides as diffusion needs to proceed through the boride shell. The aluminide finally dissolves and leaves a cell of liquid inside the boride shell of approximately the peritectic composition.

The peritectic reaction takes place to form α-aluminum and growth occurs from there. Although this theory seems to fit experimental results, but there is strong evidence against it especially by Johnsson (1993).

2.3.4.3 Hypernucleation Theory

This theory was proposed by Jones (1985) and named as such because of the disproportionate effect that very small amounts of titanium and boron make to the grain size of aluminum. Jones (1988) proposes that melt solutes segregate stably to the melt inoculants interface, and in the right conditions stable pseudocrystals can be created above the principal liquidus of the melt, and immediately below the melt liquidus these pseudocrystals allow α-aluminum to grow without undercooling. The atomic size of the segregant relative to aluminum is the key factor. Competitive segregation of solutes of mismatching size can 'poison' the otherwise hypernucleative processes. The main problem with this theory is that there is no experimental evidence.

2.3.4.4 Duplex Nucleation Theory

Of all the mechanisms proposed so far, duplex nucleation theory is the most recent and was first proposed by Mohanty and Gruzleski (1995) and further by Schumacher and Greer (1994a). Mohanty *et al* (1995) added synthetic TiB_2 particles to the aluminum melt at various titanium concentrations. It was found that $TiAl_3$ layer formed on the TiB_2 particles at hyperperitectic concentrations of Ti and α-aluminum was found on $TiAl_3$ layer.

Schumacher and Greer (1994a) added Al–Ti–B grain refiner to an aluminum rich metallic glass of composition $Al_{85}Ni_5Y_8Co_2$ and also found that borides were surrounded by $TiAl_3$ layer which was further surrounded by α-aluminum. There is a lot of criticism to the duplex nucleation theory particularly by St. John (1990).

Schumacher and Greer (1994b) suggested that an aluminide layer forms in the melt and grows at holding temperatures of 1300°C. But there is no theoretical reason for this. They suggest that at a superheat of about 740°C a stable aluminide layer forms on the surface of TiB_2 particles in the melt. At lower superheats of about 370°C they found a very thin layer of aluminide. A lot of doubt is cast on this because a high superheat not only preserves a layer of aluminide but also grows at significant holding times. Thus an aluminide layer may form during solidification. Another major problem with the duplex nucleation theory is that Johnsson and Backerud (1996) measured the nucleation and growth temperatures across the Al–Ti phase diagram for additions of Al–5%Ti–1%B master alloy and found that, at hypoperitectic composition, the nucleation temperature follows the Al–Ti liquidus curve. Duplex nucleation theory cannot explain this. The liquid adjacent to $TiAl_3$ needs to be 0.15%Ti which means that the nucleation temperature should correspond to the nucleation temperature at the peritectic concentration. This means that for an alloy containing 0.05% Ti a nucleation temperature of about 3°C higher than the liquidus temperature should be present, which the duplex nucleation theory cannot explain.

2.3.5 Fading Mechanism of Grain Refinement

There are several ways to introduce grain refiner particles into the melt. The most widely accepted method is to add commercial Al- Ti - B master alloys into the melt in the form of rod or bar. This method provides many

benefits over other methods, including emissions reduction (compared with use of salt tablets) and better composition control (Cook (1996)). However, it is important to design the addition process to achieve the most effective grain refinement, e.g. finding the contact time with the highest grain refinement efficiency (critical contact time). If the contact time is too short, the finest grain size may not be achieved. On the other hand, if the contact time is too long, effectiveness of the grain refiner will be lowered. This lower effectiveness at excessive contact time is known as fading. Many investigators (Kearns (1996)) have made an assumption that the fading time resulted from the higher density of TiB_2 and Al_3Ti, comparing to that of molten aluminum so they settled down at the bottom of the furnace after long contact time. Wang et al. (Wang (1998)) studied and observed that the composition of both Ti and B, at the top of the melt, decreased with the contact time and the resulting grain size in the casting was increased (Limmaneevichitr (2002)).

2.3.6 Growth Restriction

The degree of grain refinement relies on the balance between latent heat production and heat extraction. The rate of latent heat production is limited by the solute partitioning at the solid-liquid interface and diffusion in the melt. Partitioning is often considered for idealized binary systems in which liquidus and solidus are linear; in such a case, there is a single value for the liquidus slope m and for the solute partition coefficient k ($k=C_s/C_L$, where C_s and C_L are the solute contents of the solid and liquid in equilibrium at the interface between them). As shown, for example by Maxwell and Hellawell (1975), the diffusion-limited growth rate (d_r/d_t) of a sphere at a given melt undercooling and sphere radius, is inversely proportional to the thermodynamic quantity

$$Q = m(k-1)C_o \qquad (7)$$

where C_o is the solute content. This growth-restriction factor Q is clearly linear with solute content and for idealized systems can also be taken to be additive for different solutes in the melt. It has been shown that, in the absence of poisoning effect, Q is indeed a good parameter to describe solute effects on grain refinement for both Al-5Ti-1B and Al-3Ti-0,15C refiners (Greer (2000)). For example, Figure 4 shows that measured data for a wide range of solutes (Cr, Cu, Fe, Mg, Mn, Si, Zn and Zr) and solute addition levels fall, admittedly with some scatter, onto a universal curve of grain size vs Q for given refining conditions. Furthermore a model calculation based on titanium contents of equivalent Q provides a reasonable match to the data (Spittle (1995)). It is readily shown that the definition of Q in Eq.7 is, for small undercooling equivalent to

$$Q = -\left.\frac{dT}{df_s}\right|_{T_{liq}} \qquad (8)$$

where T is temperature, f_s the fraction solid, and T_{liq} the liquidus temperature (Dahle (1997)).

Equation (8) is useful in the calculation of Q for real systems in which the liquidus and solidus are not linear. It also permits the generalization of Q to multicomponent systems. It has long been recognized that interactions between solutes in the melt would preclude simple additivity of Q values (Dahle (1997)).

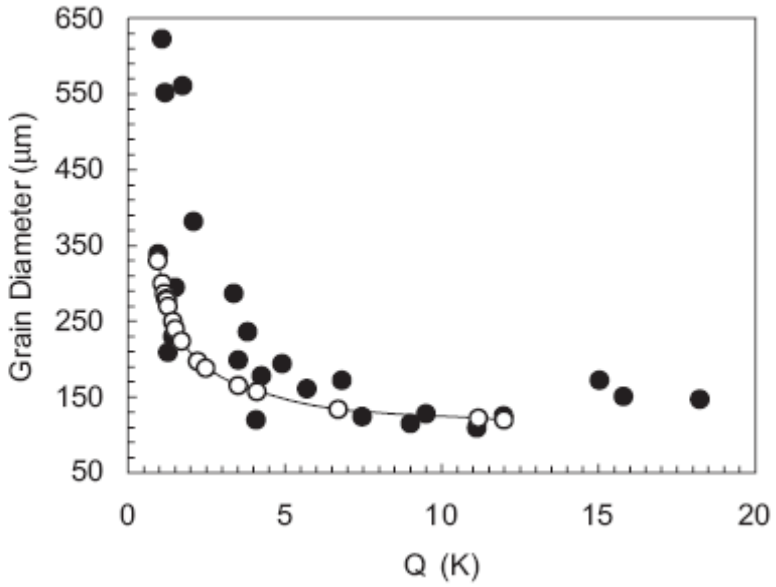

Figure 4. Grain size as a function of growth-restriction parameter Q (Eq.7) for a standard TP-1 test with 2 ppt addition of Al-5Ti-1B refiner. The measured data (●) from Spittle (1995) are compared with predictions (○) from the free-growth model (assuming an isothermal melt), taking parameters appropriate for each chosen solute (Greer (2000)).

2.4 Silicon Modification

It is standard practice to refine the eutectic structure as well as the grain structure of aluminium-silicon casting alloys. A moderate improvement in mechanical properties is guaranteed with structural integrity when the silicon eutectic phase is refined with arsenic, antimony or sulphur (Nagel (1980)). The more usual and more effective treatment is structure modification of the silicon phase, although on occasion there may be an increased susceptibility to porosity. Modification occurs naturally at rapid solidification rates typical of sand casting (impurity modification). Elements in group I and IIa and the rare earths europium, lanthanum, cerium, praseodymium, and neodymium modify, but only sodium and strontium

produce a strong modifying action at the low concentration required for commercial application. Both modifying actions transform the flake eutectic silicon into a fibrous form, producing a composite-like structure with increased ultimate tensile strength, ductility, hardness, and machinability (Davis (1994)).

2.4.1 The Solidification of Silicon

Of the two phases which take part in the freezing of an Al-Si eutectic, it is the silicon phase which plays the critical role in modification. In fact, our knowledge to date indicates that the aluminum solid solution exerts only a very mirror influence on the process. Silicon is a nonmetal, and as such freezes in what is called a faceted manner, i.e., it forms crystals which are bounded by definite crystallographic planes, and it is usually able to grow in only certain very specific crystallographic directions (Gruzleski (1999)).

The unmodified plate-like form of silicon exhibits the crystallography illustrated in Figure 5. This crystal can grow easily only in the <112> direction, and when the crystal structure of silicon is taken into account, this implies that the large flat faces of the crystal are <111> planes. A very important feature of silicon crystallization is that twins are easily formed. These crystallographic defects, occur when large groups of atoms uniformly shift position across a plane in the crystal structure, known as a twin plane. In silicon, twins form readily across the <111> planes, and this has the effect of producing a self-perpetuating groove of 141 degrees at the solid liquid interface (Figure 5). These steps originate at the twins, and due to the twining interface, there is a constant supply of growth sites at which freezing of silicon can occur. Silicon fibers are very crystallographically imperfect, and each surface imperfection is a potential site for branching to occur should it be required by the solidification

conditions. As a result, fibers in the chemically modified eutectic are able to bend, curve and split to create a fine microstructure; the plates of the unmodified structure are inhibited by their relative crystallographic perfection and can do little but form in a coarse acicular fashion (Gruzleski (1999)).

This remarkable difference in twin density is caused by the addition of only a fraction of one weight-percent modifier. One possible explanation for the effect is that atoms of the modifier absorb onto the growth steps of the silicon solid-liquid interface. If the modifier atom radius has the correct size with respect to the atomic radius of silicon ($r_{modifier}$: $r_{silicon}$=1.646) a growth twin will be caused at the interface. This phenomenon has been named, impurity induced twinning, and it is supported by the observation that modifiers become concentrated in the silicon, not the aluminum phase (Gruzleski (1999)).

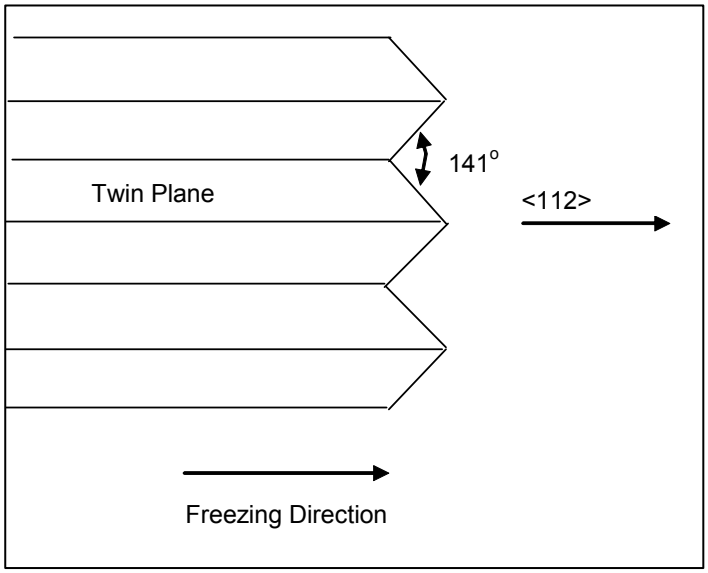

Figure 5. Schematic representation of the growth of an acicular silicon crystal from the melt

2.4.2 Quench Modification

A fibrous eutectic structure can be obtained by the rapid solidification in the growth rate range 400 to 1000 μm per second. Quench modified structures appear optically identical to impurity modified material. However, electron microscopy has revealed that the silicon is similar to the unmodified form in that it contains no, or very low, levels of twinning. This structure is simply an exceedingly fine form of the unmodified eutectic occasioned by very rapid solidification (Gruzleski (1999)).

It is well known that chemical modifiers are more effective at higher freezing rates. For example, it is much easier to modify a chill casting than a heavy section sand casting. This is to be regarded as fundamentally different from quench modification. In the presence of a chemical modifier, both the twinning frequency and the angle of branching increase with freezing rate. Both of these promote modification and lead to finer structure (Gruzleski (1999)).

2.4.3 Chemical Modifiers

The addition of certain elements, such as calcium, sodium, strontium, and antimony to hypoeutectic aluminum-silicon alloys results in a finer lamellar or fibrous eutectic network (www.key-to-metals.com).

There is, however, no agreement on the mechanisms involved. The most popular explanations suggest that modifying additions suppress the growth of silicon crystals within the eutectic, providing a finer distribution of lamellae relative to the growth of the eutectic (www.key-to-metals.com).

The results of modification by strontium, sodium, and calcium are similar. Sodium has been shown to be the superior modifier, followed by strontium and calcium, respectively. Each of these elements is mutually compatible so that combinations of modification additions can be made without adverse effects. Eutectic modification is, however, transient when artificially promoted by additions of these elements (www.key-to-metals.comT).

Antimony has been advocated as a permanent means of achieving structural modification. In this case, the modified structure differs; a more acicular refined eutectic is obtained compared to the uniform lacelike dispersed structures of sodium, calcium, or strontium-modified metal. As a result, the improvements in castability and mechanical properties offered by this group of elements are not completely achieved. Structural refinement is obtained that is time independent when two conditions are satisfied. First, the metal to be treated must be essentially phosphorus free, and second, the velocity of the solidification front must exceed a minimum value approximately equal to that obtained in conventional permanent mold casting. Antimony is not compatible with other modifying elements. In cases in which antimony and other modifiers are present, coarse antimony-containing intermetallics are formed that preclude the attainment of an effectively modified structure and adversely affect casting results (www.key-to-metals.com).

Modifier additions are usually accompanied by an increase in hydrogen content. In the case of sodium and calcium, the reactions involved in element solution are invariably turbulent or are accompanied by compound reactions that by their nature increase dissolved hydrogen levels. In the case of strontium, master alloys may be highly contaminated with hydrogen, and there are numerous indications that hydrogen solubility is increased after alloying (www.key-to-metals.com).

For sodium, calcium, and strontium modifiers, the removal of hydrogen by reactive gases also results in the removal of the modifying element. Recommended practices are to obtain modification through additions of modifying elements added to well-processed melts, followed by inert gas fluxing to acceptable hydrogen levels. No such disadvantages accompany antimony use (www.key-to-metals.com).

Calcium and sodium can be added to molten aluminum in metallic or salt form. Vacuum-prepackaged sodium metal is commonly used. Very low sodium concentrations (approximately 0.001 %) are required for effective modification. More typically, additions are made to obtain sodium content in the melt of 0.005 to 0.015 %. Remodification is performed as required to maintain the desired modification level (www.key-to-metals.com).

Strontium is currently available in many forms, including aluminum-strontium master alloys ranging from approximately 10 to 90 % Sr and Al-Si-Sr master alloys of varying strontium content (Sokolowski (2001)). A much wider range of strontium concentrations is in use. In general, addition rates far exceed those required for effective sodium modification.

A range of 0.015 to 0.050 % is standard industry practice. Normally, good modification is achievable in the range of 0.008 to 0.015 % Sr**.** Remodification through strontium additions may be required, although retreatment is less frequent than for sodium (Sokolowski (2001)).

To be effective in modification, antimony must be alloyed to approximately 0.06 %. In practice, antimony is employed in the much higher range of 0.10 to 0.50 % (www.key-to-metals.com).

2.4.4 Effects of Modification on the Microstructure

The microstructure change from acicular to fibrous silicon is not sharp one and castings with an inadequate amount of either sodium or strontium will exhibit a mixed structure-one containing regions of fibrous silicon, lamellar silicon and acicular silicon. Modification with strontium is often less uniform than with sodium and of course antimony will produce only a lamellar and never a fibrous structure (Gruzleski (1999)).

Formation of the very fine structure, sometimes called supermodified is not well understood at present. It can be produced in laboratory by rapid quenching of partially solidified samples, and although it is sometimes observed in commercial castings, its production seems to be non-repeatable (Gruzleski (1999)).

In assessing the efficiency of modification, it is sometimes useful to quantify the microstructure. This can be readily accomplished by examining a polished section under a microscope and assigning to each class the proportion of the sample surface which has a particular type of modification (Gruzleski (1999)).

Five variables determine the exact microstructure which will form:

i) type of modifier used;
ii) impurities present in the melt;
iii) amount of modifier used;
iv) freezing rate;
v) Silicon content of the alloy.

These five variables interact in a highly complex manner, and our present state of knowledge is insufficient to allow an exact quantitative prediction of microstructure, say by modification rating, for any specific set of the five (Gruzleski (1999)).

2.4.5 Overmodification

Overmodification with sodium can take place if the sodium concentration exceeds 0.018% to 0.020%. Then, a coarsening of the silicon occurs associated with bands of primary aluminum. What appears to happen at these high sodium levels is a rejection of sodium in front of the solidifying interface. The compound AlSiNa can form, and this serves to nucleate the coarse silicon particles. After some growth of silicon occurs, the adjacent liquid is aluminum rich, and a sudden nucleation and growth of aluminum then takes place which envelopes the coarse silicon and leads to the appearance of an overmodification band in the final cast product (Gruzleski (1999)).

Two distinct phenomena are associated with strontium overmodification. One of these is a coarsening of the silicon structure and the reversion of the fine fibrous silicon to an interconnected plate form. This effect has been little studied and the reasons for its occurrence are unknown. A second evidence of strontium overmodification is the appearance of strontium containing intermetallic phases in the microstructure, such as the Al_4SrSi_2 particles. It is clear that both of these effects will reduce the properties of the alloy causing them to revert to values more typical of untreated material. Interestingly, the very limited knowledge available on this subject indicates that these two effects need not occur simultaneously, i.e., Al_4SrSi_2 can occur without appreciable silicon coarsening and vice versa (Gruzleski (1999)).

2.5 Hydrogen in Aluminum

Hydrogen is the only gas that is appreciably soluble in aluminum and its alloys. Its solubility varies directly with temperature and the square root of pressure. Actual liquid and solid solubilities in pure aluminum, just above and below the solidus are 0.65 and 0.034 mL/100g respectively. These values vary slightly with alloy content. During the cooling and solidification of molten aluminum, dissolved hydrogen in excess of the extremely low solid solubility may precipitate in molecular form, resulting in the formation of primary and/or secondary voids (Davis (1994)).

Hydrogen bubble formation is strongly resisted by surface tension forces, by liquid cooling and solidification rates, and by an absence of nucleation sites for hydrogen precipitation such as entrained oxides. Dissolved hydrogen concentrations significantly in excess of solid solubility are therefore required for porosity formation. In the absence of nucleating oxides, relatively high concentrations (of the order of 0.30 mL/100g) are required for hydrogen precipitation. No porosity was found to occur in a range of common alloys at hydrogen concentrations as high as 0.15 mL/100g (Davis (1994)).

2.5.1 Hydrogen sources

There are many potential sources of hydrogen in aluminum, including the furnace atmosphere, charge materials, fluxes, external components, and reactions between the molten metal and the mold (Davis (1994)).

2.5.2 Hydrogen Porosity

Two types or forms of hydrogen porosity may occur in cast aluminum. Of greater importance is interdendritic porosity, which is encountered when hydrogen contents are sufficiently high that hydrogen rejected at the solidification front results in solution pressures above atmospheric. Secondary (micron-size) porosity occurs when dissolved hydrogen contents are low and void formation is characteristically subcritical (Davis (1994)).

2.5.3 Hydrogen Removal (Degassing)

Dissolved hydrogen levels can be reduced by a number of methods. The simplest is to hold the metal at a lower temperature for some period of time during which the hydrogen solubility is lower and thus provide for natural outgassing. Casting conditions that permit solidification with natural expulsion of hydrogen without the attendant porosity are also desirable. However, neither of these is always possible. Deliberate degassing of the melt can be accomplished in the following ways:

i) Gas purging or gas flushing
ii) Tableted flux degassing
iii) Mechanical mixer degassing (Davis (1994)).

2.5.3.1 Gas Purging

One of the degassing methods is by injecting a purging gas or gas mixture under pressure through a flux tube, pipe, lance or wand. A purge gas

serves to collect hydrogen because of the lower partial pressure of the hydrogen afforded by the collector bubbles versus the surrounding melt. Hydrogen diffuses into the purge gas bubble, which rises to surface of the melt and is expelled into the atmosphere. Purge gas can be either inert (argon or nitrogen) or reactive (chlorine and Freon 12). Reactive gases are used in small concentrations of under 10% along with an inert gas. Reactive gases undergo an actual chemical reaction with the melt. Chlorine reacts with molten aluminum to form a gaseous $AlCl_3$, which then serves as the purging gas. In the case of Freon, fluorine reacts to form AlF_3, a solid phase. Both chlorine and fluorine have very favorable effects on bubble surface tension and in wetting out inclusions from the melt (Molland (1979)).

2.5.3.2 Vacuum Fluxing

In large melts, a series of alloys were refined using argon fluxing for 30 minutes through porous plugs. Pressure was maintained at 7 Pa. Hydrogen contents were reduced from 0.16 to 0.11 ppm. 0.24 to 0.12 ppm and 0.17 to 0.13 ppm for the three alloys respectively. One particular advantage of vacuum fluxing is the minimal amount of dross formed (Aarflot (1985)).

2.5.3.3 Hexachloroethane Degassing

Perhaps the most common method of degassing in foundry applications is the use of hexachloroethane (C_2Cl_6) tablets. The tablets decompose in the aluminum melt to form gaseous $AlCl_3$. The rising $AlCl_3$ gas bubbles then collect hydrogen gas and deliver the gas to the melt surface for release (Clegg (1986)).

The tablets may also contain salt fluxes to help wet oxide inclusions within the melt and thus enable some removal of the hydrogen gas associated with inclusions (Clegg (1986)).

2.5.3.4 Rotary Degassing

The use of simple gasses or gas mixtures in lance or flux tube degassing, although reasonably effective, is not necessarily full efficient. The ability of this simple process to degas depends on the bubble size generated and the amount of contact area between the degassing bubbles and the melt. The bubbles are often large, and very little mixing occurs in large melts or vessels when flux tubes or lances are used (Kissling (1963)).

The principle of the rotary injector system is that gas is injected into the column or shaft of a rotating member and is released through five openings at the base or rotor. When rotating at speeds of 300 to 500 rpm, the disperser shears the incipient gas bubble released, producing a wide dispersion of very fine bubbles for degassing (Snow (1987)).

The high surface area-to-volume ratio of degassing bubbles provides greatly increased reaction kinetics resulting in more efficient degassing. The level of hydrogen removal depends on gas flow rate and initial hydrogen content as well as metal flow rate, but most commercial systems can achieve final hydrogen contents well below 0.15 mL/100g (Snow (1987)).

2.6 Thermal Analysis

The solidification of a pure metal or an alloy is accompanied by the evolution of heat (latent heat of fusion), the magnitude of which depends on the various phases that form during freezing. If one measures the temperature of a solidifying alloy, the temperature-time plot that is so obtained can yield useful information about how the alloy freezes. Such a plot is called a cooling curve and the general name given to the technique is thermal analysis (Tenekedjiev (1995)).

A pure metal, such as aluminum, freezes at a unique temperature (660.6°C) and so the cooling curve exhibits a plateau at this temperature. Freezing starts at the beginning of the plateau when latent heat is no longer given off. Solid solution alloys freezes over a range of temperatures rather than at a single temperature. Their cooling curves show only slope changes when solidification begins or ends. Binary eutectic alloys, such as the exact Al-Si eutectic composition, freeze at a single well-defined temperature much like a pure metal. Their cooling curves are therefore similar to those of pure metals, with the temperature of the plateau indicating the freezing temperature. The cooling curves of hypo- or hyper eutectic alloys have a characteristic form. Freezing of the primary phase takes place over a range of temperatures and is associated with slope changes. Eutectic solidification follows primary freezing and the cooling curve also exhibits a plateau that ends when solidification is complete. The most important departure arises because solidification reactions do not begin exactly at the equilibrium freezing temperature. It is usually necessary for the temperature to drop below the equilibrium value before freezing begins. This phenomenon is known as undercooling. As soon as solidification commences, latent heat is given off and the temperature rises to, or close to, the equilibrium value. This is known as recalesence. Any solidification process may exhibit undercooling and recalesence. If the

quantity of heat associated with a reaction is too small or is taken away too rapidly, it is quite possible that no recalesence will be observed on the cooling curve. In such a case the temperature for that reaction is observed to occur will be less than the true equilibrium temperature for that reaction. This becomes an increasingly important consideration as the cooling rate of the thermal analysis sample increases. At high cooling rates heat loss from the sample is great that the latent heat cannot bring the sample temperature anywhere near equilibrium. All temperature determined from such a cooling curve can be far less than equilibrium and reactions that involve only a small fraction of the total sample volume may not appear at all on the cooling curve. It is evident that cooling curves taken at slow freezing rates are more accurate and yield more information than those obtained under conditions more rapid solidification (Tenekedjiev (1995)).

It should be evident that the cooling curve becomes more complex as the alloy complexity increases. Real foundry alloys are far from simple binary alloys. Their solidification behavior is characterized by a series of reactions involving two or more solid phases (Tenekedjiev (1995)).

In addition, primary solidification of aluminum is always observed, and the formation of primary iron-bearing phases can sometimes be seen (Tenekedjiev (1995)).

Major phase changes are usually obvious on a cooling curve, but depending on the composition, some of the minor reactions may be hardly visible. In order to reveal the exact temperatures at which such reactions occur, it is normal to employ a derivative curve. In such curve, the slope of the cooling curve (dT/dt) is plotted as a function of time. Small changes in the slope of the cooling curve appear as obvious peaks on the derivative curve (Tenekedjiev (1995)).

2.6.1 Thermal Analysis Equipment

Several devices for the thermal analysis of aluminum alloys are available commercially. These consist of a sampling cup, a microcomputer for data acquisition and analysis, and appropriate software. The sampling cup is of a simple design, a thermocouple is fixed in the center of the cup with the mid-point. Cups are either shell-molded sand or thin-walled steel, with a shell molded sand base. In either case, solidification is relatively slow, requiring 6-8 minutes (Gruzleski (1999)).

A major difference between the various testers lies in the approach to the analysis of the cooling curve. Some use a complex algorithm to assess the microstructure, while others employ only a single parameter. In all cases, however, information on the grain size and extent of eutectic modification can be obtained. Analysis of the cooling curve is performed automatically by the microcomputer, and the operator is presented with the results of this analysis in a simple form (Gruzleski (1999)).

2.6.2 Thermal Analysis Control of Grain Refinement

Conventional techniques consisting of visual examination of the grain structure are time consuming. Thermal analysis provides a reliable and rapid method of evaluating the nucleation potential of the melt prior to pouring the castings. It can result in the use of lower amounts of refiners to maintain a fine-grained structure (Apelian (1984)).

The nucleation potential of the melt may be correlated to undercooling on the liquidus arrest of the cooling curve of a solidifying sample taken form the melt. When an insufficient number of nuclei is present (low nucleation potential), solidification will start after an important degree of undercooling.

If an abundance of nucleation sites is present (high nucleation potential), little or no undercooling takes place. This is illustrated in Figure 6 (Apelian (1984)).

A better indication of grain size, particularly at coarser sizes, can be obtained by taking into account the period of apparent supercooling. This is useful because at large grain sizes, the undercooling may not be large, but it tends to last for an extended period of time. This is due to the time factor required for nucleation (Gruzleski (1999)).

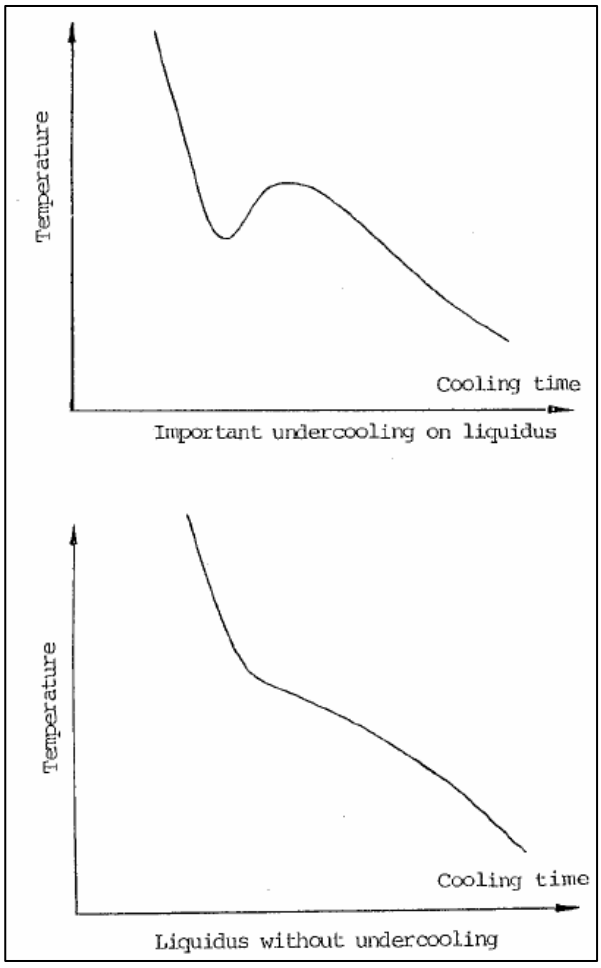

Figure 6. Relation between undercooling and nucleation potential

2.6.3 Thermal Analysis Control of Eutectic Modification

When an alloy is modified, three features of the cooling curve may be changed:

i) the temperature of the eutectic plateau,
ii) the undercooling required to start eutectic freezing,
iii) time duration of this undercooling.

These are indicated schematically in Figure 7. With modification, the eutectic temperature is depressed, the undercooling for nucleation of the eutectic is increased, and the period of this undercooling lengthens (Gruzleski (1999)).

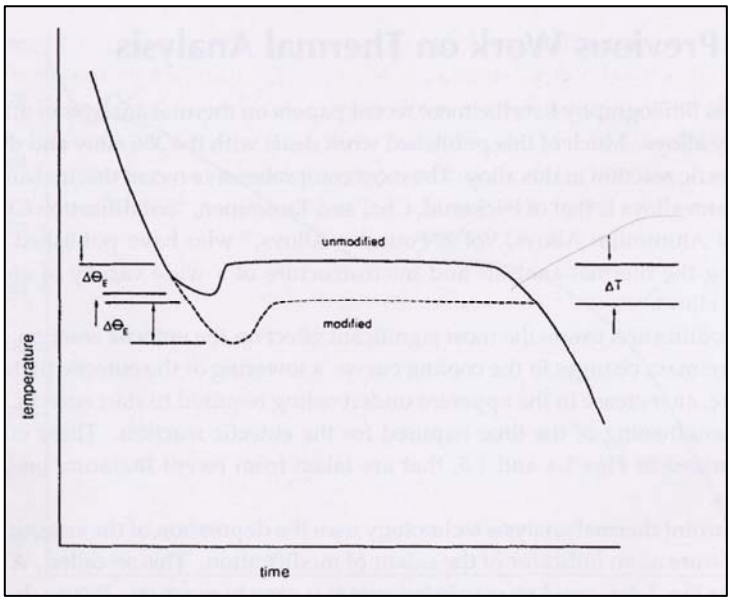

Figure 7. A comparison of the eutectic regions of the cooling curves of modified and unmodified alloys.

The feature most used in thermal analysis control of modification is the depression of the eutectic temperature. Since the eutectic temperature is easy to measure, it is often employed by foundries to assess whether or not a melt is properly modified. This quantity is usually called the ΔT (Gruzleski (1999)).

More sophisticated approaches to modification control are possible and are useful in some circumstances. If temperature alone is used as the criterion for proper modification, it is not very easy to detect overmodified to modified transition. Consideration of the undercooling required to start eutectic freezing can, however, be used. With modification, the undercooling $\Delta\theta_E$, increases and then falls off as structure becomes modified. Values for overmodification are considerably lower than those found with unmodified structures, and so it is possible to distinguish between the two (Argyropoulos (1983)).

CHAPTER 3

EXPERIMENTAL PROCEDURE

3.1 Material and Processing

The $AlSi_9Mg$ alloy was used as the test alloy, $AlTi_5B$ was used as the grain refiner and Sr was used as the modification agent in the experiments. To prepare $AlSi_9Mg$ alloy, aluminum Al99,7(DIN) and pure Si and pure Mg were used. The chemical composition of the Al99,7(DIN) is given in Table 1.

Table 1. Chemical composition of Al99,7 (DIN)

	Cu %	Fe%	Si%	Zn%	Ti%
Al99.7 (DIN)	0.03	0.25	0.15	0.04	0.03

Nine different alloys were prepared by changing the Ti weight percentage from 0.04% to 0.15% and Sr weight percentage from 0.013% to 0.017%. The aim of preparing these nine alloys was to find the optimum amount of Ti and Sr to obtain fine grain size and good modification. The chemical compositions of the alloys are given in Table 2.

Table 2. Weight percentages of materials in the alloys

Alloy Name	Si%	Fe%	Cu%	Mn%	Mg%	Zn%	Ti%	Sr%
Alloy I	7.3	0.05	0.02	0.02	0.6	0.08	0.04	0.013
Alloy II	7.3	0.05	0.02	0.02	0.6	0.08	0.08	0.015
Alloy III	7.3	0.05	0.02	0.02	0.6	0.08	0.15	0.017
Alloy IV	7.3	0.05	0.02	0.02	0.6	0.08	0.15	0.015
Alloy V	7.3	0.05	0.02	0.02	0.6	0.08	0.15	0.013
Alloy VI	7.3	0.05	0.02	0.02	0.6	0.08	0.08	0.013
Alloy VII	7.3	0.05	0.02	0.02	0.6	0.08	0.04	0.015
Alloy VIII	7.3	0.05	0.02	0.02	0.6	0.08	0.04	0.017
Alloy IX	7.3	0.05	0.02	0.02	0.6	0.08	0.08	0.017

Two different alloying and casting procedure were used, the aim of these two different procedures was to find the effect of degassing method to the grain refinement and modification, and these procedures were:

First Procedure:

1) Melting of pure aluminum
2) Addition of pure Si
3) Addition of Sr (via AlSr10)
4) Addition of Ti (via AlTi5B)
5) Sampling for Thermal analysis at different time intervals
6) Gravity die casting for mechanical test specimens

Second Procedure:

1) Melting of pure aluminum
2) Addition of pure Si
3) Addition of Sr (via AlSr10)
4) Addition of Ti (via AlTi5B)

5) Degassing (Using Hexaflorethane)
6) Sampling for Thermal analysis at different time intervals
7) Gravity die casting for mechanical test specimens

To find the optimum contact time after mixing the Ti and Sr into the melt, sample was spooned from the melt and poured into the disposable thermal analysis cup of the Alu-Therm instrument at 15., 30., 45. and 60. minutes. And at the same time the tensile test specimens were also poured by gravity die casting.

In addition to standard casting sequence, for some alloys sand casting was done to see the mechanical properties difference between the sand casting and gravity die casting. For this aim sand molds were prepared, each for casting two bars of dimensions 280 mm in length and 28 mm in diameter.

3.2 Equipment

Ajax Magnethermic coreless induction furnace was used for melting the $AlSi_9Mg$ alloys with prepared amounts of $AlTi_5B$ as a grain refiner and $Al_{10}Sr$ as a modifier. To obtain cooling curves and thermal analysis data from the molten metal, Alu-Therm system was used, which is the aluminum thermal analyzer of the Heraeus Electro-Nite. Alu-Therm thermal analyzer system contains:

1) Shell-molded sand cup for sampling
2) Holder
    a) Contact Block
    b) K-Type extension wires
3) Instrument
    a) Lap-top PC

b) Alu-Therm software
c) Measurement module which converts mV to °C.

3.2.1 Sampling Cup

Heraeus Electro-Nite thermal analysis cups for aluminum thermal analysis were used (Figure 8 and 9). These thermal analysis cups contain K-Type (NiAl – NiCr) thermocouple, which is positioned vertically to measure temperature from the middle of the sample. Thermocouple wires are ceramic insulated except for the top of the wires to measure the temperature just from the middle of the sample, also these NiAl – NiCr wires are turned around each other to improve accuracy.

Figure 8. Thermal analysis cup for aluminum

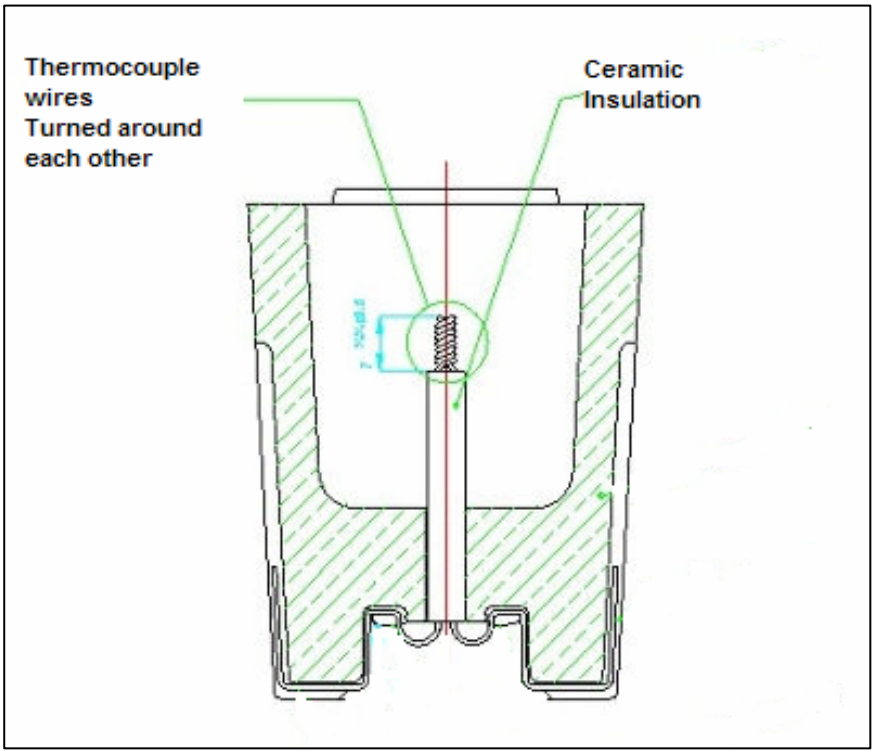

Figure 9. Schematic drawing of thermal analysis cup

3.2.2 Holder

Holder contains contact block and extension wire (Figure 10). By means of contact block, thermocouple signal is sent to the measurement module of the Alu-Therm system through extension K-Type compensation wire.

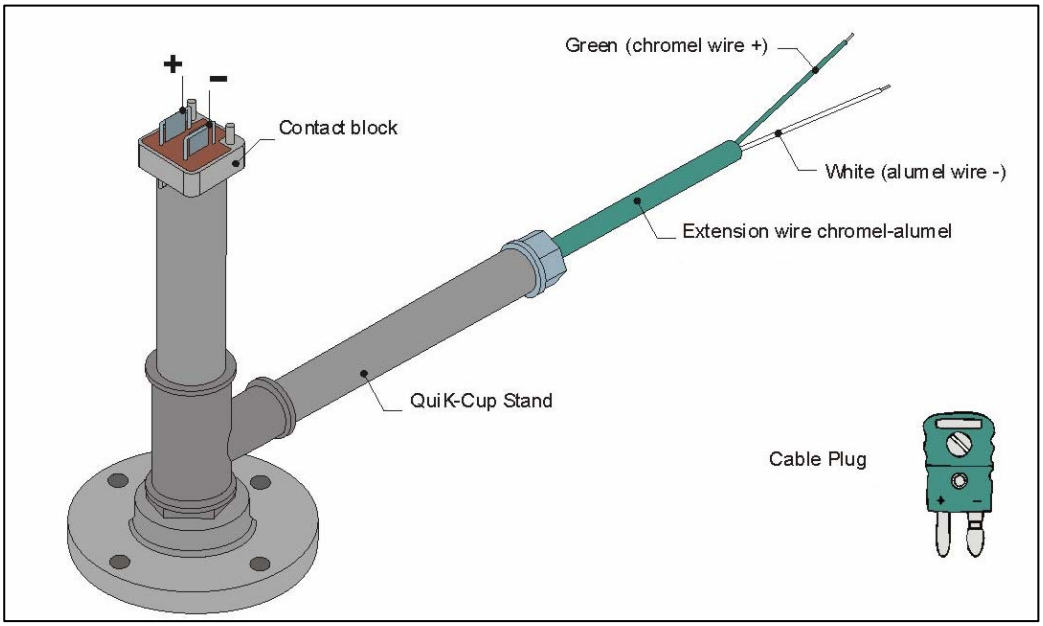

Figure 10. Holder of the Alu-Therm system

3.2.3 Instrument

The thermocouple signal is converted from mV to °C in the measurement module by the electronic unit in it, which has room temperature compensation and has an autocalibration capability (Figure 11).

When the signal is converted to °C, it instantaneously comes to the Alu-Therm software and this software begins to draw temperature profile with corresponding time to obtain cooling curve (Figure 12).

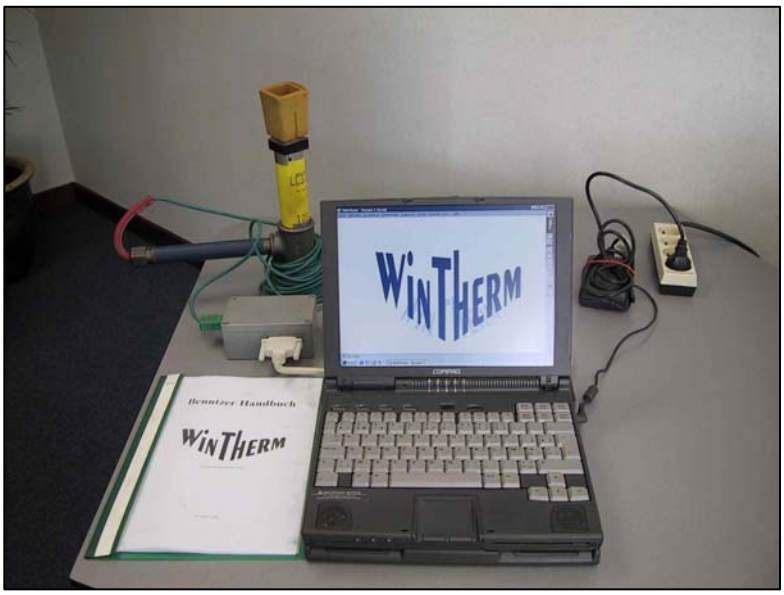

Figure 11. Alu-Therm System

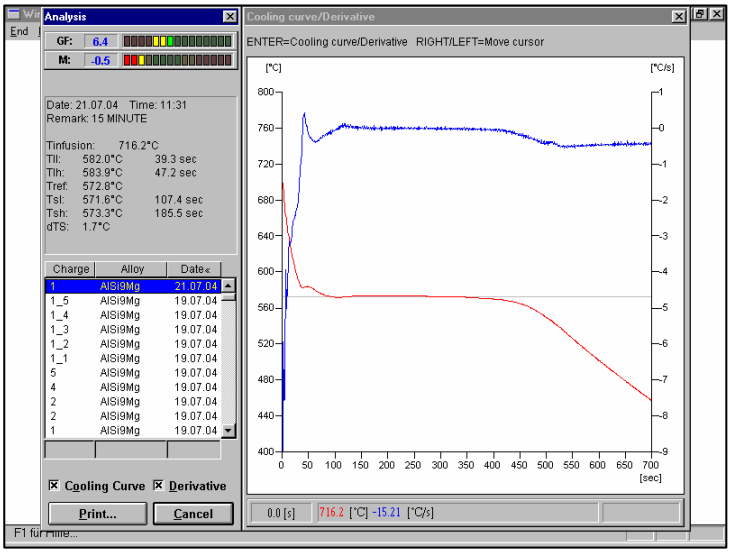

Figure 12. Alu-Therm software screen

3.3 Specimen Preparation

3.3.1 Metallographic Examination of Specimens

Specimens taken from the end of the tensile test specimens were prepared for metallographic examination. Samples were firstly grounded with 120, 240, 400, 600, 800 and 1200 grid sandpapers and then samples were polished with alumina of 1 micron particle size.

To measure the dendrite arm spacing, polished samples were etched by Keller's reagent which contains 2.5% HNO_3, 1.5% HCl, 1% HF and 95% H_2O. The dendrite arm spacing of the specimens were measured by the image analyzer with the help of Clemex software. At the end, representative photographs were taken by a digital camera.

For grain size measurements, specimens were etched by a reagent which was prepared by mixing 100 ml H_2O, 200 ml HNO_3, 180 ml HCl and 60 gr $FeCl_3$.

3.3.2 Tensile Test Specimens

The die cast and sand cast bars were machined to reduce the diameter of the middle part to obtain standard tensile test specimens. The dimensions of the tensile test specimens are shown in Figure 13.

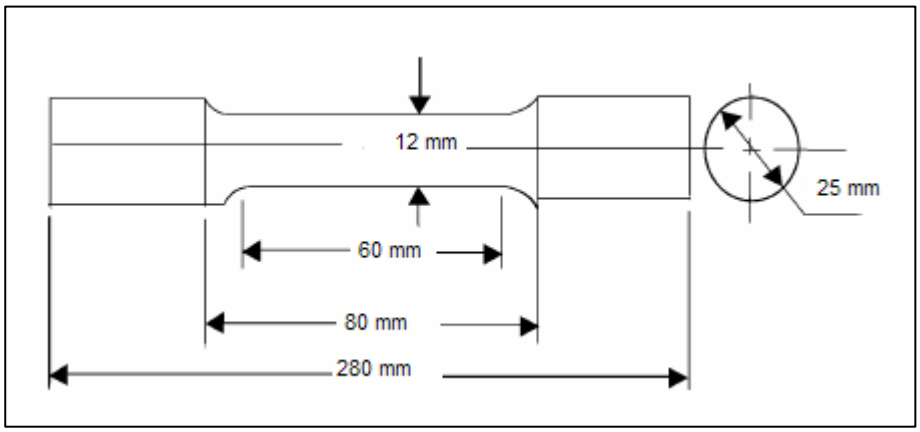

Figure 13. Dimensions of the tensile test specimen

3.4 Experiments

3.4.1 Metallographic Examinations and Image Analysis Studies

Microstructures of cast samples were examined by metallographically to see the effect of grain refinement, modification and contact time to the microstructure.

To see the grain refinement and contact time effect to the primary aluminum phase, the alloys with different amounts of grain refiner were cast at different contact times. And then they were analyzed by the image analyzer to measure secondary dendrite arm spacings. And at the end, representative photographs were taken by a digital camera.

The grain count was carried out by the line intercept method as it was mentioned in the ASTM E 112-88 standards. The number of grains per cm was obtained by drawing a 1 cm line across the sample, and then the number of grains intersecting the line was counted. And then this number was converted to the number of grains per cm^2 to find amount of grains in per area.

3.4.2 SEM Study

In order to get detailed information about of the contact time after the addition of grain refiner, TiB_2 plate like morphologies were studied by SEM microscope with JSM-6400 Electron Microscope (JEOL), equipped with Noran system. Also percentages of alloying elements were analyzed and their graphs were obtained.

3.4.3 Tensile Tests

The mechanical strength of the alloys was determined by tensile testing. To obtain ultimate tensile strengths of the machined tensile test specimens, Alşa tensile testing machine was used, which has a capacity of 60 tons. The testing machine had a transmitting slidewire to provide an electrical signal proportional to the load applied for digital illustration purpose.

3.4.4 Hardness Tests

Brinell Hardness Test was done to determine the hardness values of the specimens. Brinell hardness values were obtained by using a Heckert macro hardness tester. All tests were performed with 2.5 mm diameter ball under 15,3 kg loads.

3.4.5 Fading Test

To find the effect of waiting time to the grain refiner efficiency $AlSi_9Mg$ alloy was prepared, with 0.22% Ti. The sand mold was prepared to obtain 4 cylindrical samples and molten metal was poured to the sand molds after 15, 30, 45 and 60 minutes to find the exact fading time. To perform macroexamination and SEM analysis all samples were cut in half along the longitudinal axes and from this sample two different samples were cut out both from bottom and top. The picture of the sand mold is given in Figure 14 and dimensions of the cylinders are given in Figure 15.

Figure 14. Picture of the sand mold for cylindrical samples

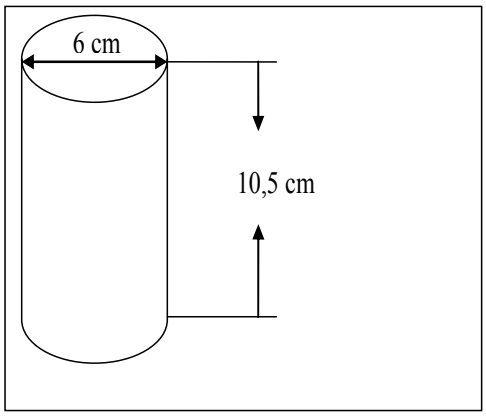

Figure 15. Dimensions of the cylindrical samples

CHAPTER 4

EXPERIMENTAL RESULTS AND DISCUSSION

4.1 Experimental Results

In this study, thermal analysis parameters of a series of $AlSi_9Mg$ alloy were examined and correlation of these parameters to microstructure and mechanical properties was determined.

4.1.1 Thermal Analysis Results

To see the effect of grain refiner and modifier, the parameters of the aluminum thermal analysis and the alloy's cooling curve characteristics with the help of first derivative curves were obtained. The definition of these parameters is given in Table 3. And the values of these parameters for the 9 different alloys at different times are given in Appendix A.

Table 3. Parameters of the Alu-Therm thermal analyzer

GF	Grain Refinement Parameter
M	Amount of Modification
Tinf	Initial Temperature at the crucible
Tll	Lowest temperataure at the liquidus
Tll time	The second when the lowest temperature at the liquidus occurs
Tlh	Highest temperature at the liquidus
Tlh time	The second when the highest temperature at the liquidus occurs
Tref	Eutectic temperature of the unmodified alloy
Tsl	Lowest temperature at the solidus
Tsl time	The second when the lowest temperature at the solidus occurs
Tsh	Highest temperature at the solidus (Eutectic Temperature)
Tsh time	The second when the highest temperature at the solidus occurs
dTs	Amount of undercooling at the solidus
ΔT(L)	Amount of undercooling at the liquidus
ΔT length	Length of the liquidus undercooling as a second
dTs length	Length of the solidus undercooling as a second

4.1.2 Metallographic Examination Results

The microstructures of the specimens were examined metallographically to see the effect of different amounts of added grain refiner and modifier. Since the cooling rate is so fast in the die cast specimens, grain size could not be measured due to the dendritic solidification morphology. The secondary arm spacing (DAS) of these specimens were measured instead of grain size. The results of DAS measurements of the die cast specimens are given in Table 4. Examples of the measured dendrite secondary arm spacing from the microstructures is given in Figure 16 (a) and (b).

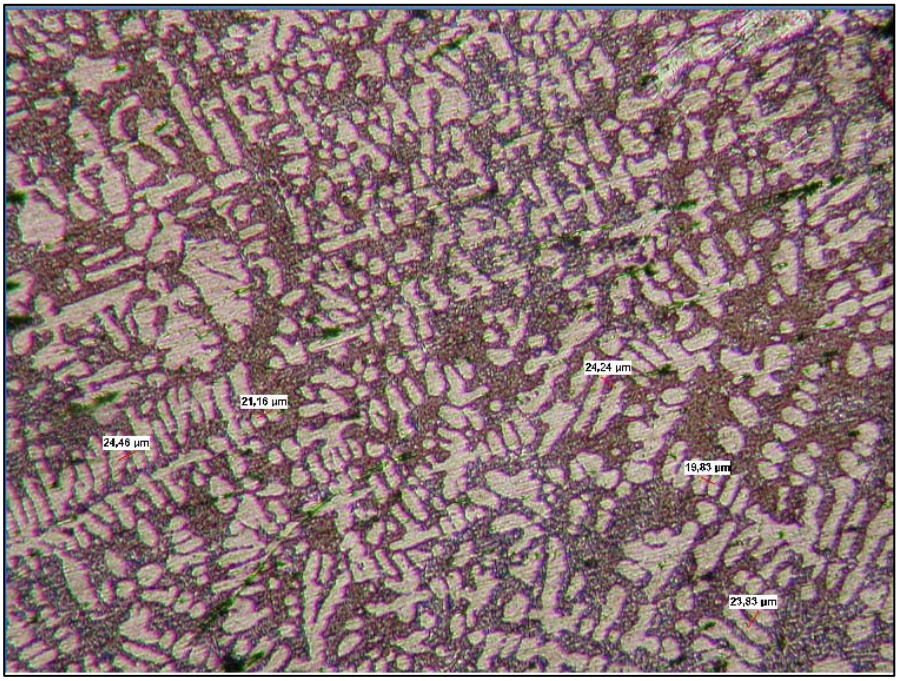

(a)

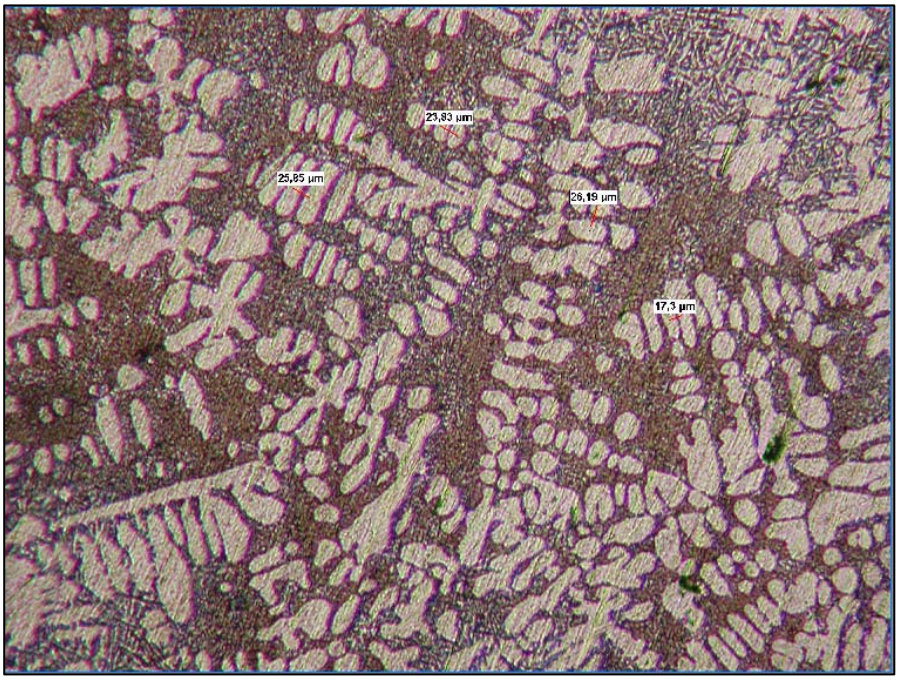

(b)

Figure 16. (a) and (b) dendrite secondary arm spacing measurement by image analyzer

Table 4. Dendrite Secondary Arm Spacing of the Die cast specimens

Alloy Name	Fading Time (min)	(DAS) Dendrite Arm Spacing (µm)
Alloy I	15 min	20,54
	30 min	14,56
	45 min	18,61
	60 min	15,35
Alloy II	15 min	24,83
	30 min	17,81
	45min	25,59
	60 min	22,45
Alloy III	15 min	28,23
	30 min	25,30
	45 min	21,72
	60 min	22,99
Alloy IV	15 min	22,70
	30 min	19,30
	45min	25,73
	60 min	23,29
Alloy V	15 min	26,50
	30 min	25,80
	45 min	27,32
	60 min	25,34
Alloy VI	15 min	26,81
	30 min	23,65
	45min	34,21
	60 min	35,91
Alloy VII	15 min	34,99
	30 min	25,49
	45 min	30,94
	60 min	21,33
Alloy VIII	15 min	24,10
	30 min	20,56
	45min	29,00
	60 min	22,28
Alloy IX	15 min	27,76
	30 min	22,39
	45min	19,30
	60 min	20,81

4.1.3 Mechanical Tests Results

4.1.3.1 Tensile Test Results

The results of the tensile tests and corresponding percent elongations are given in the Table 5.

Table 5 . Tensile Test Results

Alloy Name	Fading Time (min)	UltimateTensile Strength (Mpa)	Elongation (%)
Alloy I	15 min	176,02	2,76
	30 min	135,48	2,24
	45 min	173,79	4,12
	60 min	160,19	2,90
Alloy II	15 min	181,56	-
	30 min	152,97	-
	45min	154,36	3,28
	60 min	137,15	1,06
Alloy III	15 min	181,56	-
	30 min	183,23	5,11
	45 min	182,68	-
	60 min	217,10	9,35
Alloy IV	15 min	186,01	4,70
	30 min	166,57	4,12
	45min	160,47	1,74
	60 min	180,45	3,51
Alloy V	15 min	149,15	2,70
	30 min	161,16	2,95
	45 min	174,5	2,70
	60 min	-	-
Alloy VI	15 min	216,93	4,55
	30 min	198,51	3,00
	45min	205,98	3,40
	60 min	165,16	2,90
Alloy VII	15 min	164,36	2,20
	30 min	180,1	3,00
	45 min	184,64	1,60
	60 min	185,7	3,50
Alloy VIII	15 min	195,31	5,50
	30 min	200,64	3,90
	45min	201,71	3,60
	60 min	-	-
Alloy IX	15 min	215,59	5,30
	30 min	183,57	2,30
	45min	200,11	4,50
	60 min	182,5	2,10

4.1.3.2 Hardness Test Results

Hardness test results of the die cast specimens are given in Table 6.

Table 6. Hardness Test Results

Alloy Name	Fading Time (min)	Hardness HB
Alloy I	15 min	61,3
	30 min	62,1
	45 min	57,0
	60 min	62,0
Alloy II	15 min	65,8
	30 min	61,7
	45min	61,2
	60 min	56,6
Alloy III	15 min	58,3
	30 min	59,8
	45 min	53,0
	60 min	59,3
Alloy IV	15 min	59,0
	30 min	61,2
	45min	57,1
	60 min	54,6
Alloy V	15 min	71,9
	30 min	72,8
	45 min	65,8
	60 min	62,7
Alloy VI	15 min	59,8
	30 min	60,4
	45min	60,4
	60 min	62,7
Alloy VII	15 min	59,0
	30 min	61,9
	45 min	59,0
	60 min	57,6
Alloy VIII	15 min	61,9
	30 min	61,2
	45min	60,4
	60 min	59,1
Alloy IX	15 min	63,6
	30 min	66,7
	45min	66,1
	60 min	65,0

4.1.3.3 Fading Test Results

To see the distribution of TiB_2 plate-like particles in the cylindrical samples, 2 samples were cut out from the bottom and top of the samples. SEM analysis was done to find the TiB_2 distribution. Also grain size measurement by macroexamination was done to see the effectiveness of the grain refiner. Photographs of the samples taken from both from top and bottom of the cylindrical samples poured at 15, 30, 45 and 60 minutes are given in Figure 17 and grain sizes that were measuring by the line intercept method are given in Table 7.

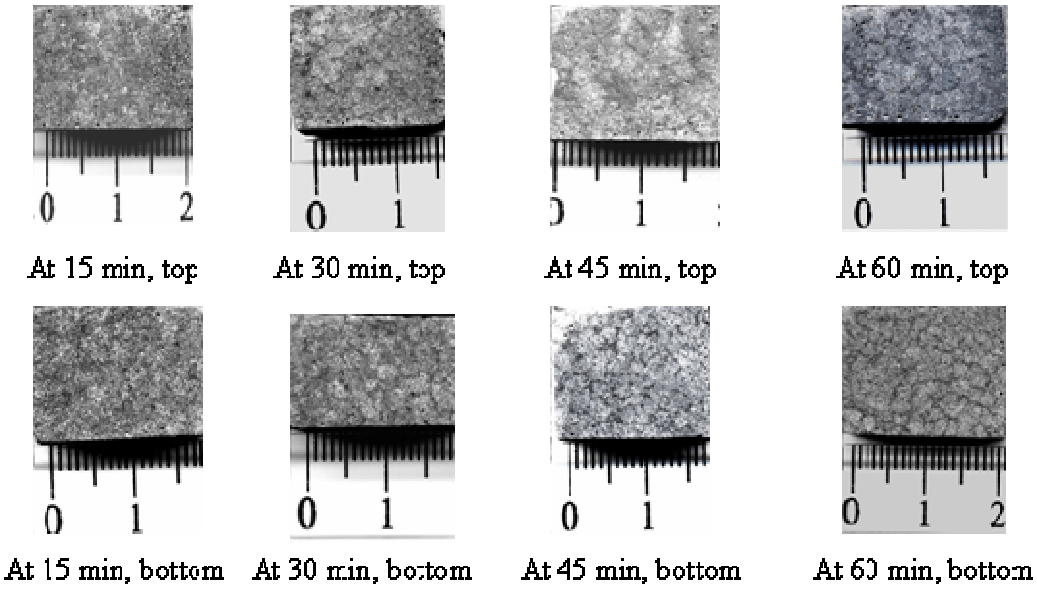

Figure 17. Photographs show the variation of grain size with time

Table 7. Grain size of the samples

Waiting time	Place	Grain Size
15 min	Bottom	25
15 min	Top	24,16
30 min	Bottom	23,04
30 min	Top	29,16
45min	Bottom	17,64
45min	Top	Dendritic
60 min	Bottom	19,36
60 min	Top	21,16

Grain sizes obtained by macroexamination are given in Table 7. And this table shows that grain sizes decrease until to 45th minute but after that time grain sizes increase again, which shows that fading mechanism occurs 45 minutes after addition of grain refiner.

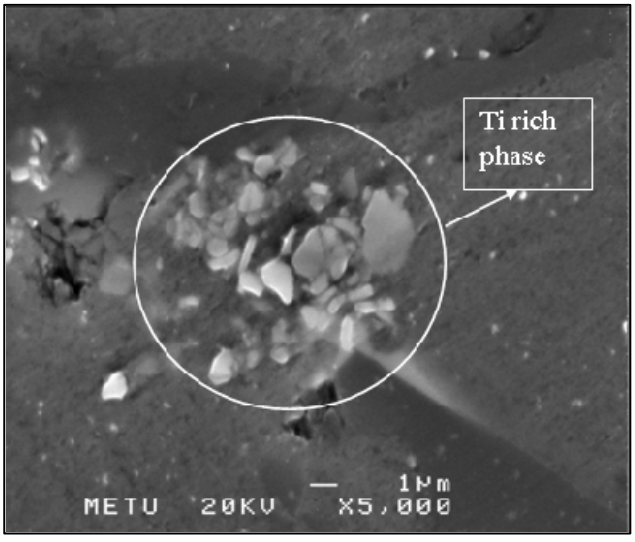

Figure 18. SEM micrograph of the sample, in which Ti-rich phase can be observed easily

The SEM analysis also shows that there are TiB_2 plates agglomerated in the structure but no relationship could be found between TiB_2 particles and grain size. Since boron could not be detected by SEM analysis Ti rich phase was found in the microstructure and this Ti-rich phase photographed by SEM microscope is given in Figure 18 and weight and atomic percentage of this phase is given in Figure 19.

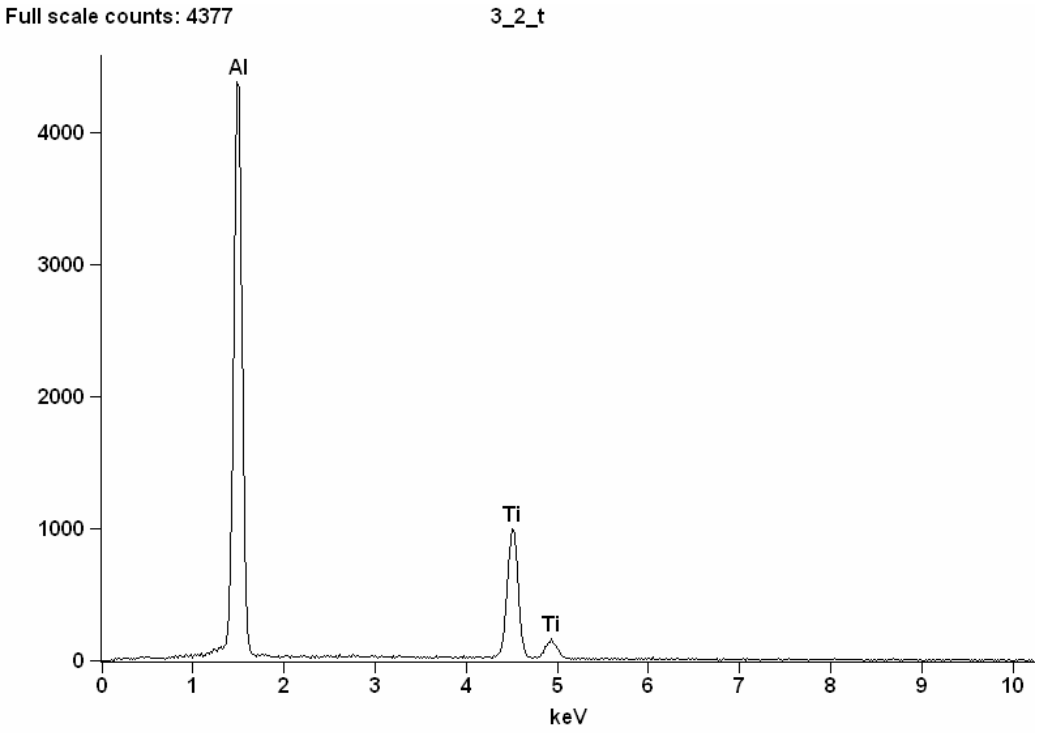

Element	*Weight Conc %*	*Atom Conc %*
Al	64.44	76.29
Ti	35.56	23.71

Figure 19. EDXA plot and elemental analysis of Ti-rich phase.

4.2 Discussion of Results

4.2.1 Effect of Ti% to the cooling curves and microstructure

Experimental results have shown that as the Ti percent increases from 0.04 to 0.15 the grain refinement factor (GF) determined by the thermal analyzer also increase, which is illustrated in Figure 20.

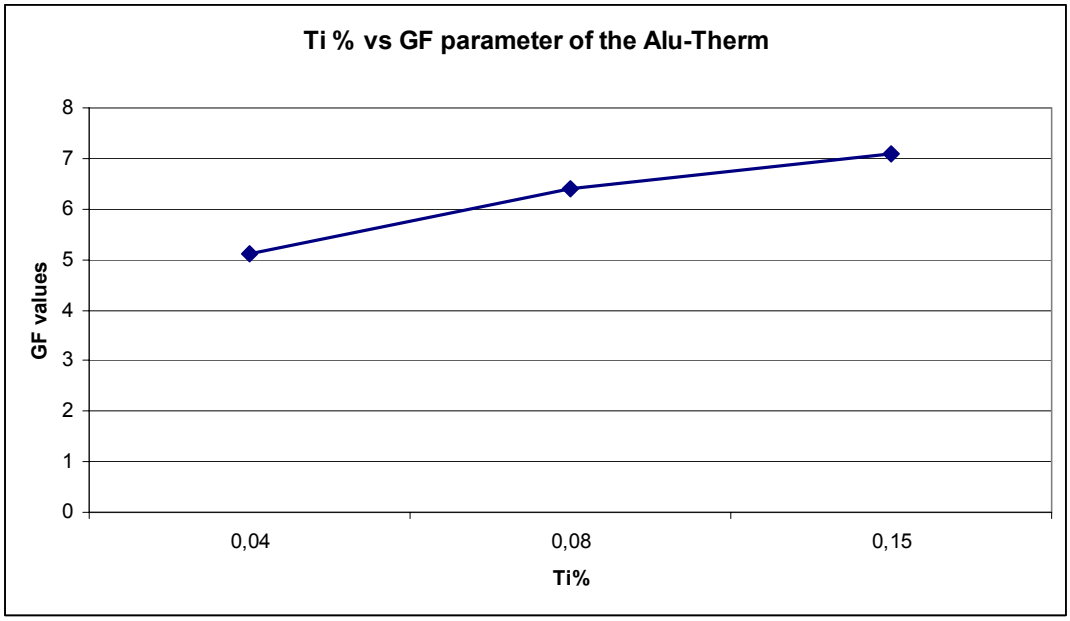

Figure 20. Graph of the GF parameter with changing amount of Ti%

And with increasing GF parameter, lowest temperature of the liquidus increases, which corresponds to TIl parameter of the thermal analyzer; this trend can be seen in Figure 21.

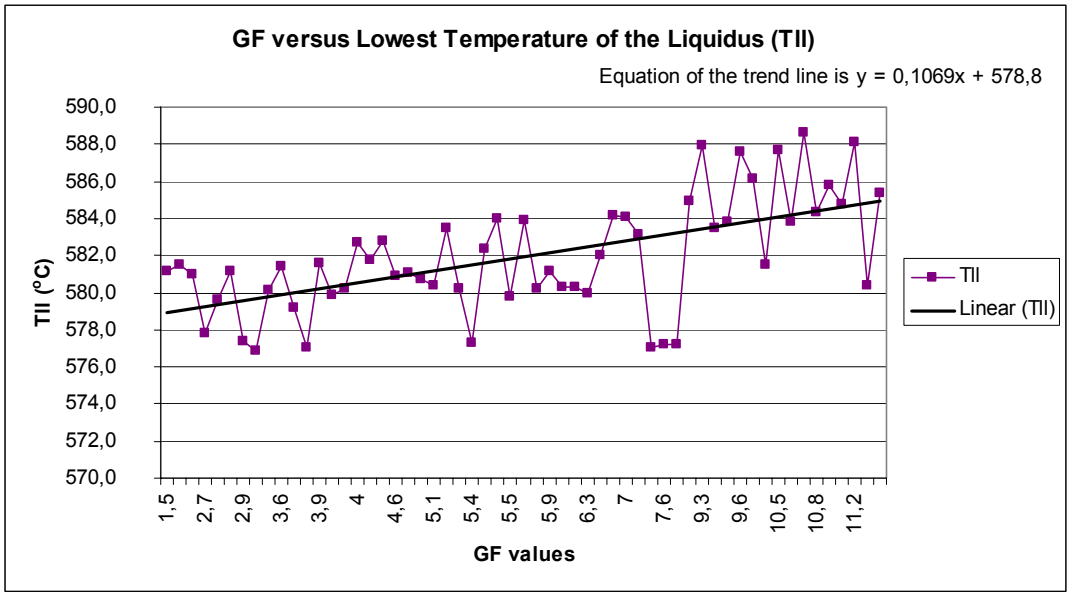

Figure 21. GF versus lowest temperature of the liquidus (Tll)

Also with increasing GF parameter highest temperature of the liquidus also increases, which corresponds to Tlh parameter. This trend is illustrated in Figure 22. However, the undercooling (ΔT) at the liquidus which is equal to ΔT = Tlh – Tll decreases with increasing GF parameter. To understand this situation the trend lines of the GF versus Tll graph and GF versus Tlh graphs were examined and the slope of these lines were calculated. From the slope it was found that the slope of the GF versus Tll is bigger than the slope of the GF versus Tlh trend line. Due to that difference in slopes, ΔT at the liquidus decreases with increasing GF factor. The relationship between ΔT and the GF parameter is given in Figure 23.

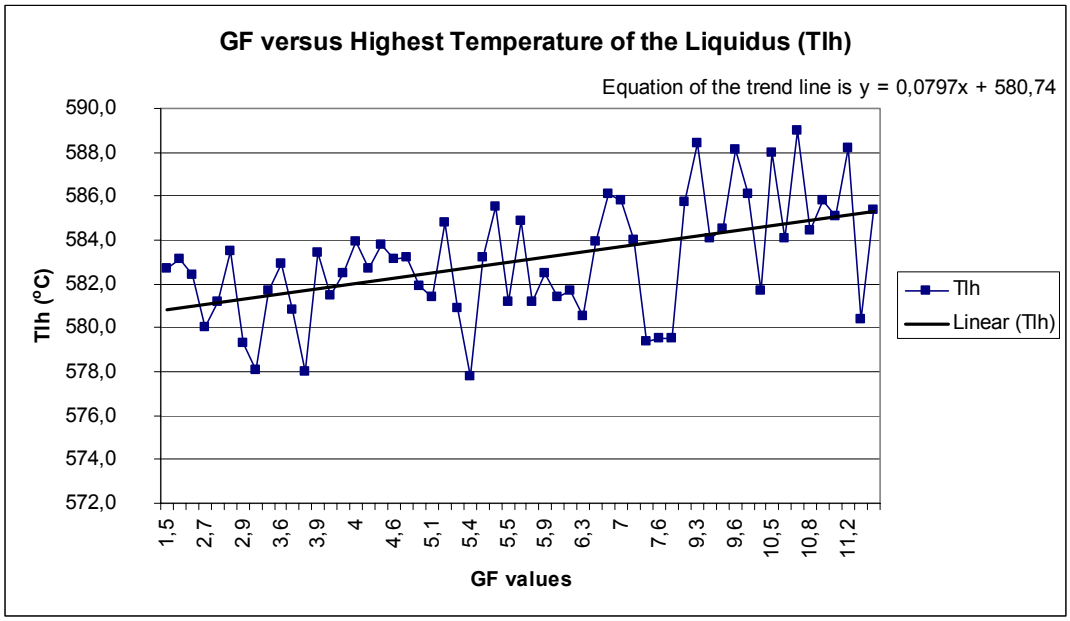

Figure 22. GF versus highest temperature of the liquidus (Tlh)

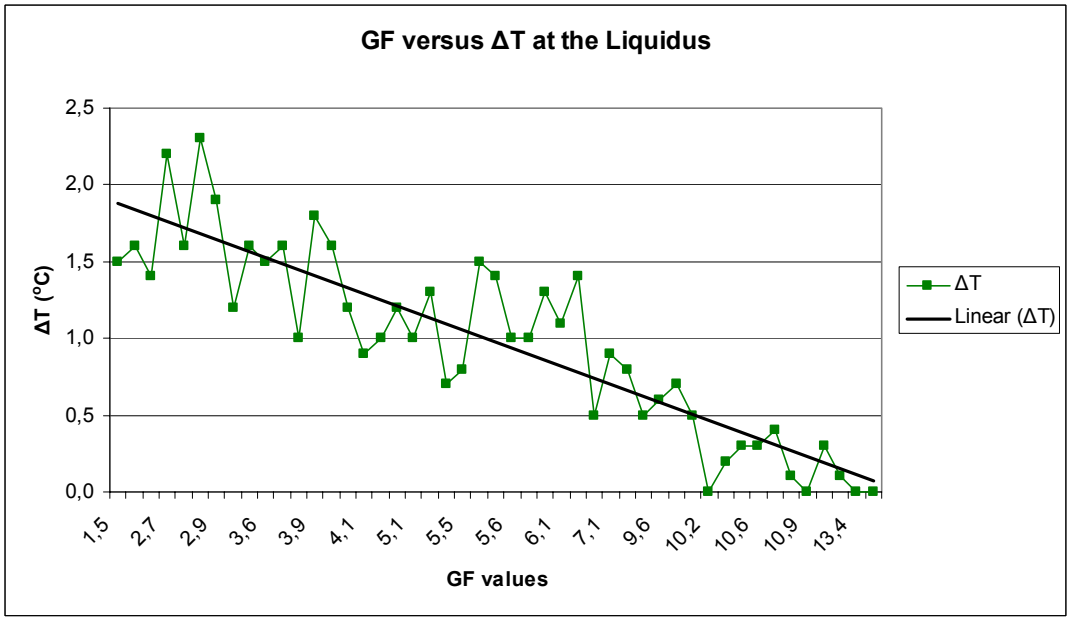

Figure 23. GF versus ΔT at the liquidus

According to the results, it is apparent that, ΔT length of the liquidus which corresponds to (Tlh time) – (Tll time) is getting narrower with GF parameter, and this relationship is given in Figure 24.

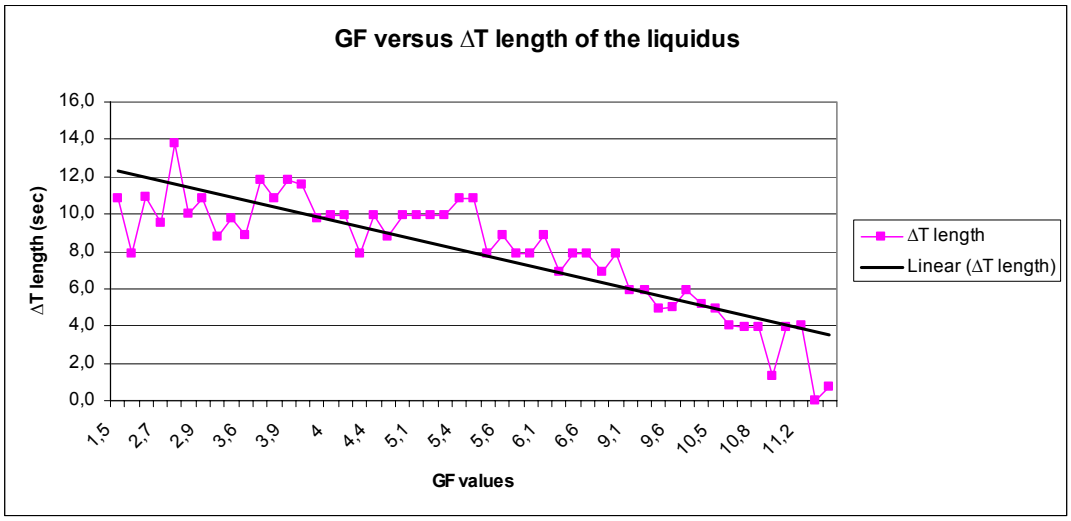

Figure 24. GF versus ΔT length of the liquidus

These relations show that as the Ti percent increases the grain refinement factor (GF), the lowest temperature of the liquidus (Tll) and highest temperature of the liquidus (Tlh) increase. On the other hand amount of undercooling (ΔT=Tlh-Tll) and length of the undercooling at the liquidus decreases. And these results are consistent with the results found in literature (Argyropoulos(1983)),(Charbonnier (1979)).

Experimental results also show that there is a relationship between the GF parameter and the initial temperature at the sampling cup which is the T_{inf} parameter of the Alu-Therm thermal analyzer. The experimentally determined GF values increase with decreasing T_{inf}, which means that

grain refinement factor (GF) is directly related with the pouring temperature. Grain size decreases with decreasing pouring temperature. The graph of this relationship is given in the figure below (Figure 25).

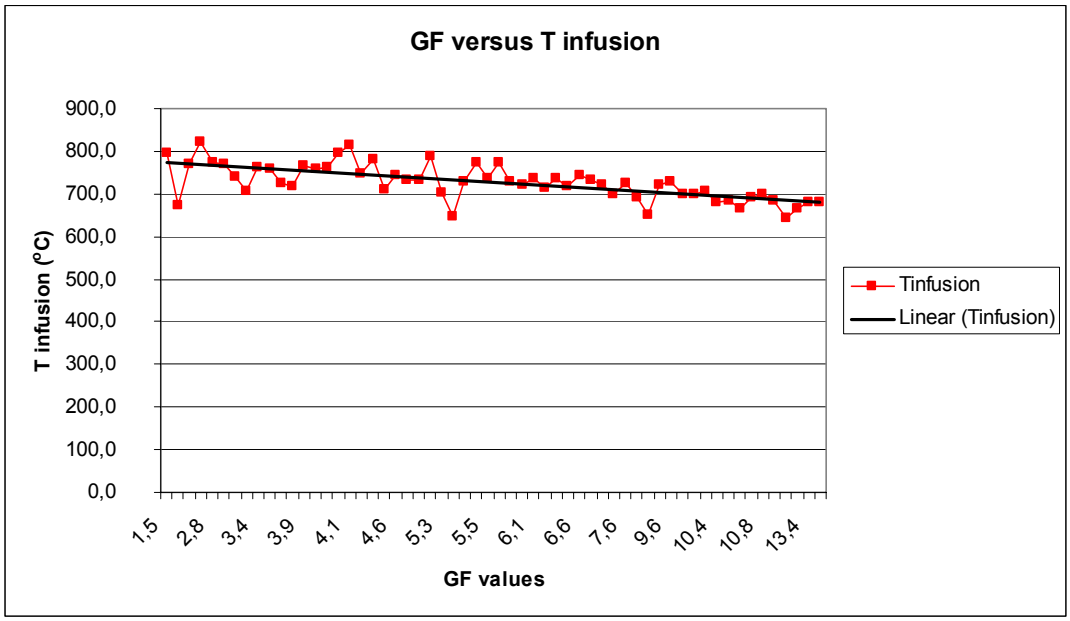

Figure 25. GF versus Initial temperature at the sampling cup (Tinf)

To see the relationship between thermal analysis parameters and final products, the dendrite secondary arm spacing and the grain refinement factor (GF) results of the thermal analyzer were compared. And the figure 26 prove that there is a direct relationship between GF values and the dendrite secondary arm spacing, also this relationship can also be understood from the comparison of the cooling curves with the microstructures as seen in Figure 27.

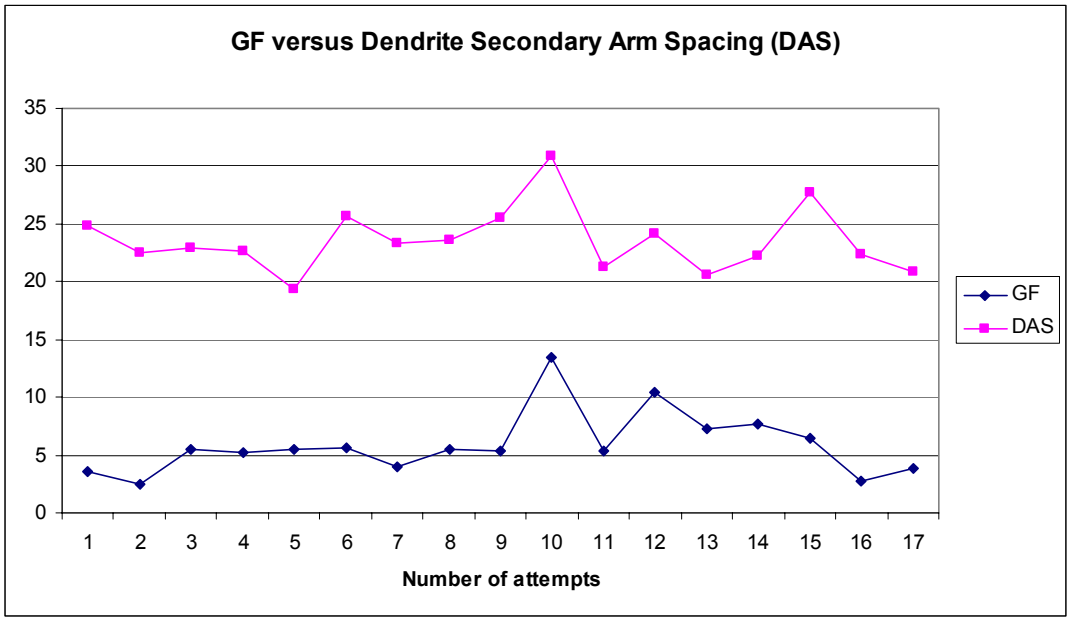

Figure 26. GF values versus Dendrite secondary arm spacing (DAS)

As it can be seen from the Figure 27, the GF factor increases with decreasing undercooling at the liquidus (first arrest at the red curve). This decreasing at the liquidus can also be understood from the first derivative curve (blue curve in the Figure 27) of the cooling curve because first derivative at the liquidus is getting sharpen as the undercooling increase. It can be concluded that the dendritic structure of the α-aluminum phase get coarsen with decreasing GF parameter which increases with undercooling.

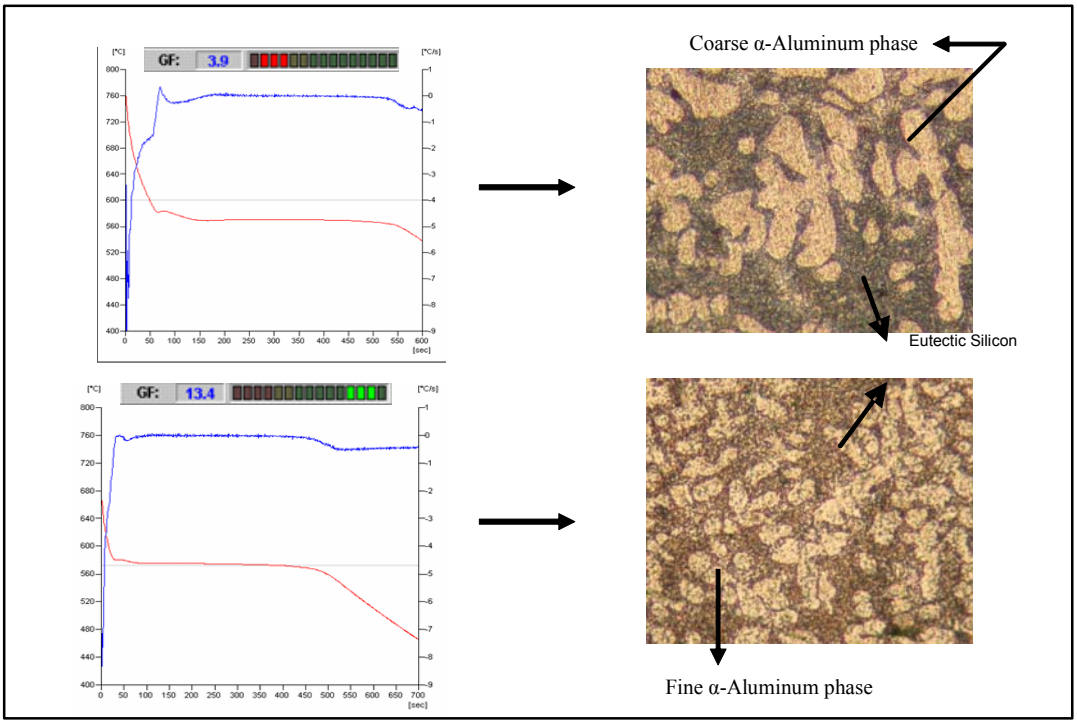

Figure 27. Comparing the cooling curves including GF results with microstructures

4.2.2 Effect of Sr percent to the thermal analysis results, microstructures and mechanical properties

Experimental results have shown that as the weight percent of Sr in the molten alloy increases from 0.013 to 0.017, the eutectic temperature of the alloy decreases. This trend can also be understood from the modification factor (M) of the thermal analyzer, since M is equal to Eutectic temperature of the unmodified alloy – Eutectic temperature of the modified alloy, M values increase as the Sr weight percent increases. The graph of this relationship is given in Figure 28.

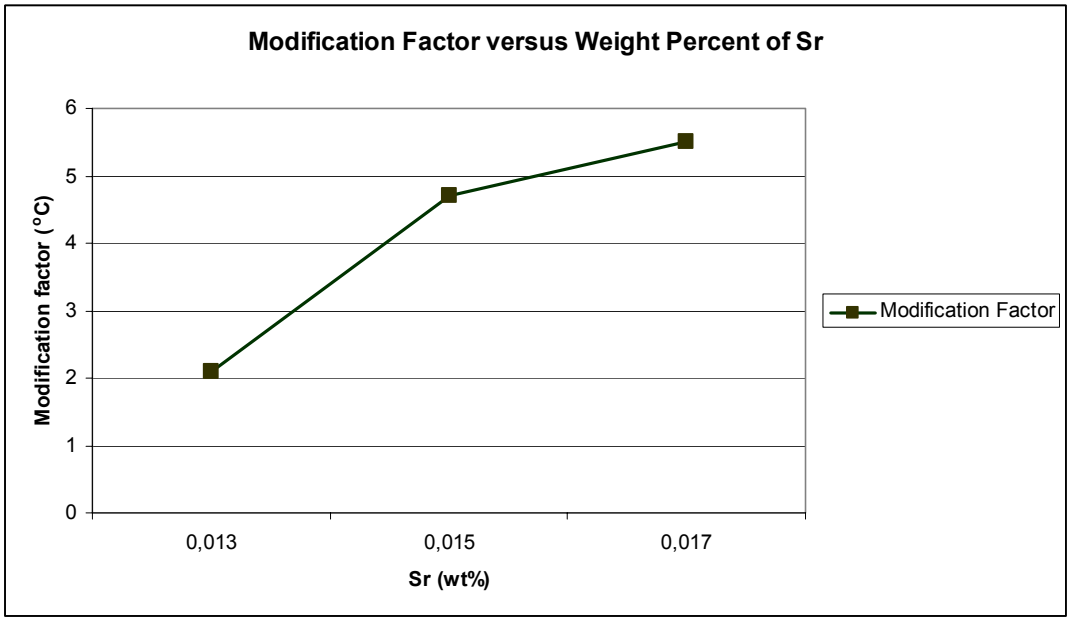

Figure 28. The graph of modification versus weight percent of Sr as an AlSr10 master alloy

To prove this relationship between modification factor (M) and the weight percent of Sr, the microstructures were also examined and they were compared to the modification factor, this comparison is illustrated in Figure 29. As it can be seen from this figure, as the modification factor (M) increases, morphology of the Si phase changes from acicular to fibrous structure.

It can be concluded that there is a relationship between Sr weight percent and the amount of undercooling at the solidus. This relationship can be understood when examining the modification factor (M) and the amount of undercooling at the solidus (dTs) which is a parameter of the thermal analysis. This relationship is illustrated in Figure 30. As it can be seen from Figure 30 the amount of undercooling increases with increasing modification factor (M).

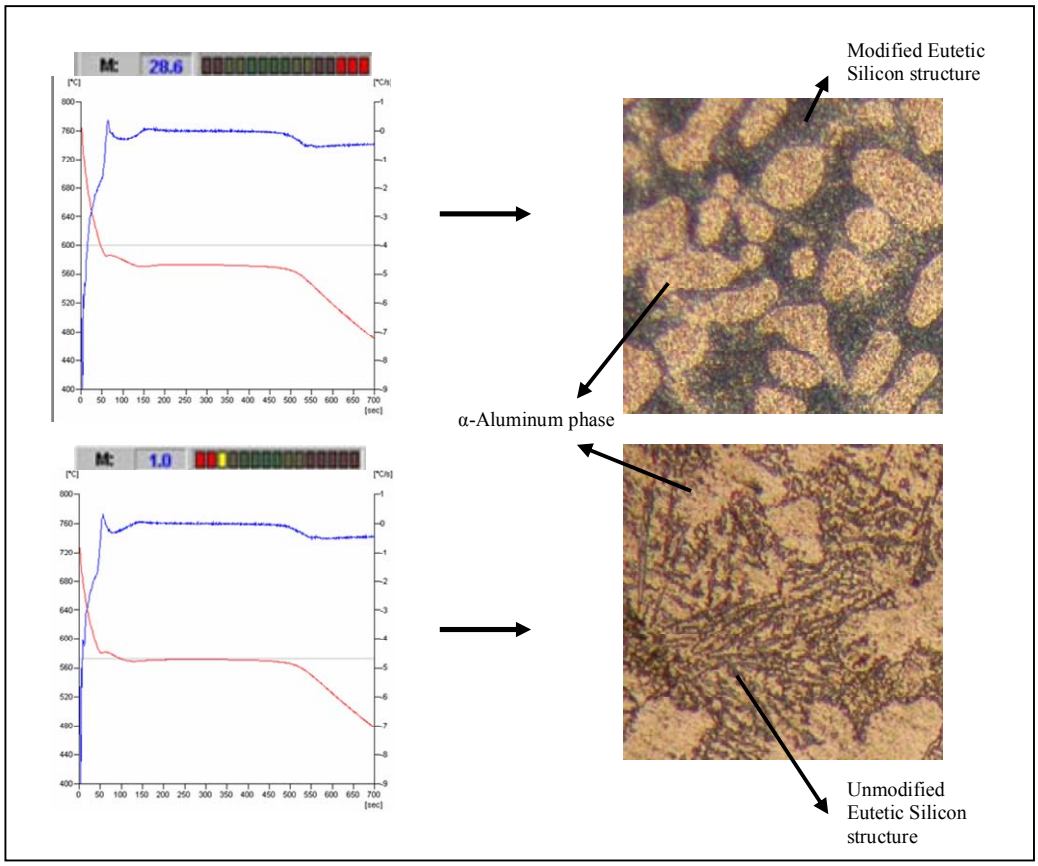

Figure 29. Comparing the cooling curves including M results with microstructures

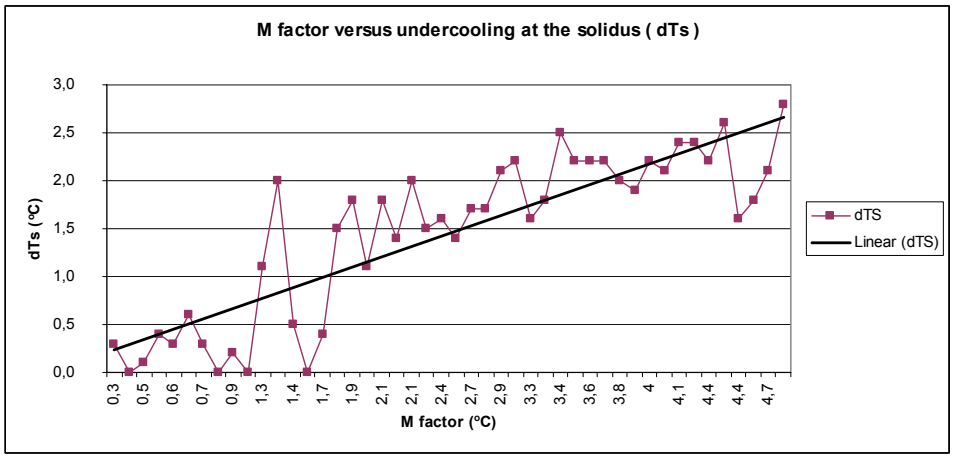

Figure 30. Modification factor (M) versus amount of undercooling at the solidus

The thermal analysis results show that as the modification increases, the length of the eutectic temperature arrest also gets longer. This relationship is given in Figure 31.

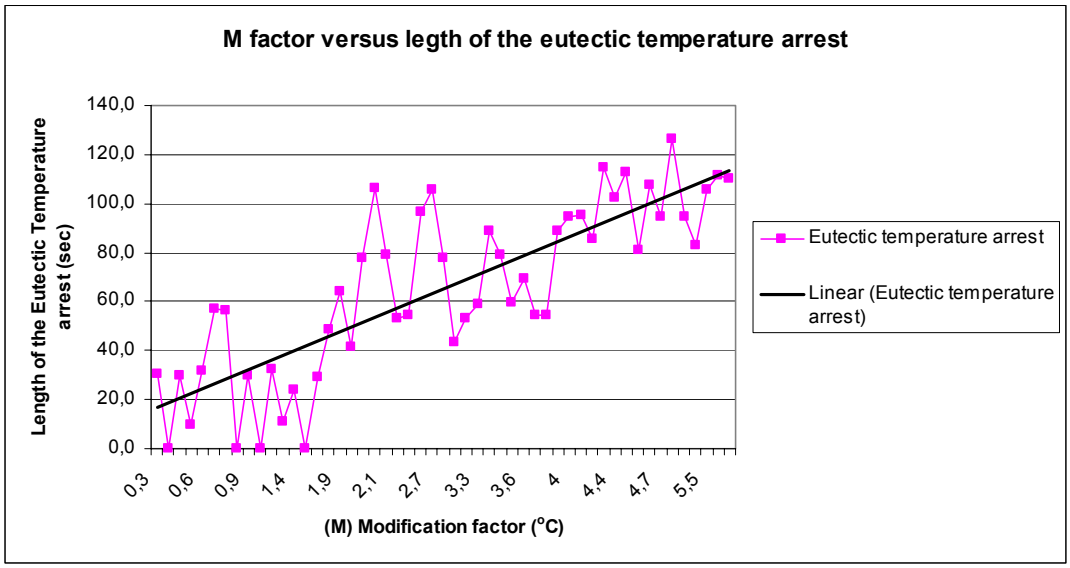

Figure 31. Modification factor versus length of the eutectic temperature arrest

These situations can be explained by this suggestion: the Sr addition restrains the growth of the eutectic silicon, which provides a finer eutectic structure, and these results are consistent with the results found in literature (Gruzleski (1999)).

According to the results, it is apparent that, the length of the eutectic temperature arrest also depends on the weight of the thermal analysis sample; this relationship is given in Figure 32. The relationship between the weight of the sample and the length of the eutectic temperature arrest can be explained as: if the time corresponds to the end of the eutectic

temperature arrest supposed to be the end of the solidification, then it can be conclude that as the mass of the molten sample increases the time that is needed to cool the sample down also increases.

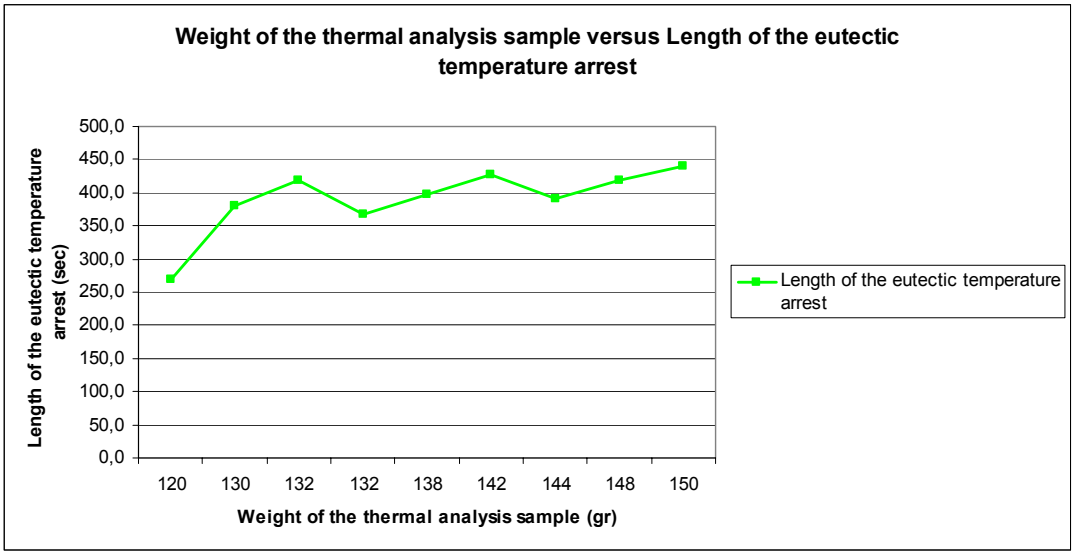

Figure 32. Comparing the cooling curves including M results with microstructures

4.2.3 Effect of waiting time to the thermal analysis parameters

Thermal analysis results have shown that waiting time after the addition of grain refiner has a great effect on the effectiveness of the grain refiner. This effect can easily be understood when examining the grain refinement factors (GF) of the thermal analysis results which belonged to different waiting times of nine different alloys. This relationship is given as a chart in Figure 33.

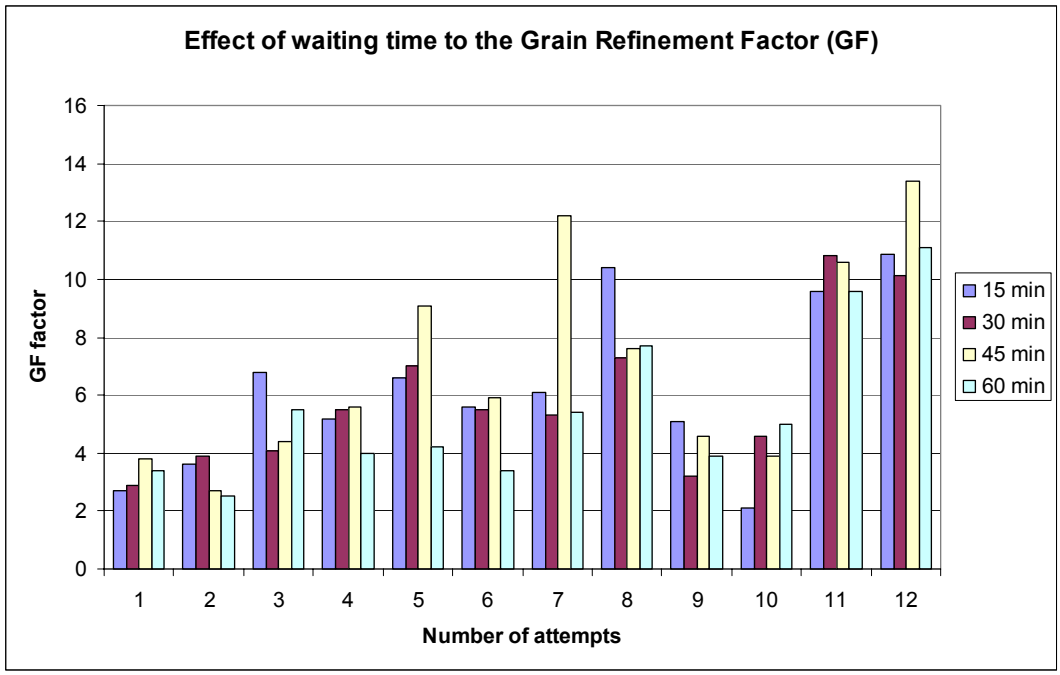

Figure 33. Effect of waiting time on the grain refinement factor

As seen in Figure 33, the grain refinement factor increases with increasing waiting time and makes a peak at the 45 minutes waiting time. After this point GF factor begins to decrease, which means that if waiting time is too short, the finest grain size may not be achieved. On the other hand, if the waiting time is more than 45 minutes, effectiveness of the grain refiner may be lowered. This lower effectiveness at excessive waiting time is known as fading. Many investigators (Kearns (1996)) have made an assumption that the fading time resulted from the higher density of TiB_2 and $AlTi_3$, compared to that of molten aluminum so they settled down at the bottom of the furnace after long waiting time. Wang et al. (Wang (1998)) studied and observed that the composition of both Ti and B, at the top of the melt, decreased with the waiting time and the resulting grain size in the casting increased (Limmaneevichitr (2002)).

4.2.4 Effect of Degassing to the thermal analysis results, microstructures and mechanical properties

Two procedures that were tried have shown that degassing by hexaflorethane chemical tablets after the addition of grain refiner and modifier reduce the effect of modifier but not grain refiner. The effect of degassing on the modifier was examined by the modification parameter of the thermal analyzer both with degassing and without degassing the same alloy and this effect can easily be seen from Figure 34.

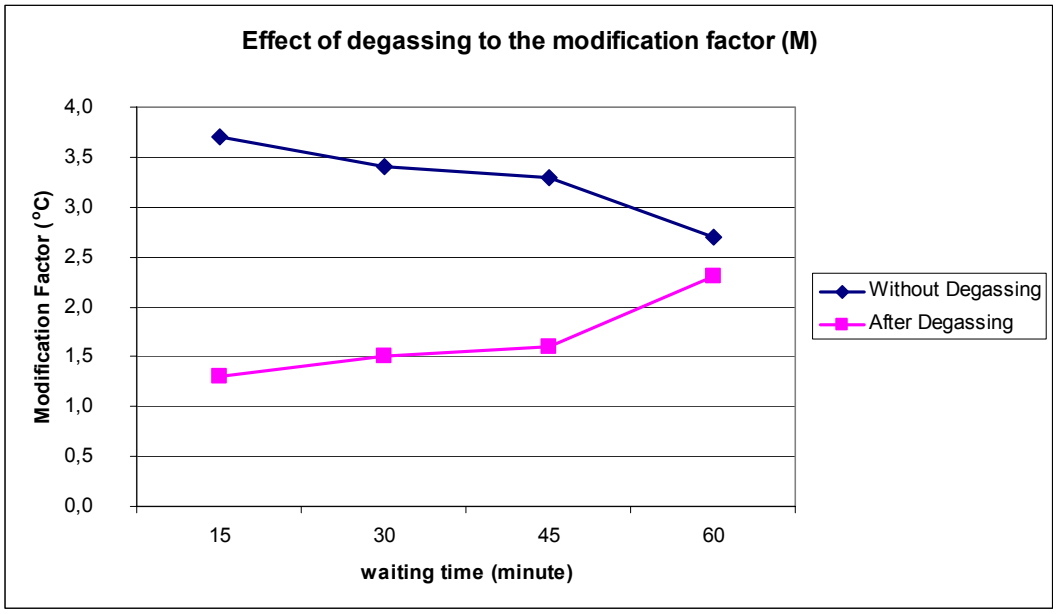

Figure 34. Effect of degassing to the modification factor

The effect of degassing on the grain refiner was examined by the modification parameter of the thermal analyzer both with degassing and without degassing the same alloy and it was found that degassing has no influence on grain refinement. This relationship is given in Figure 35.

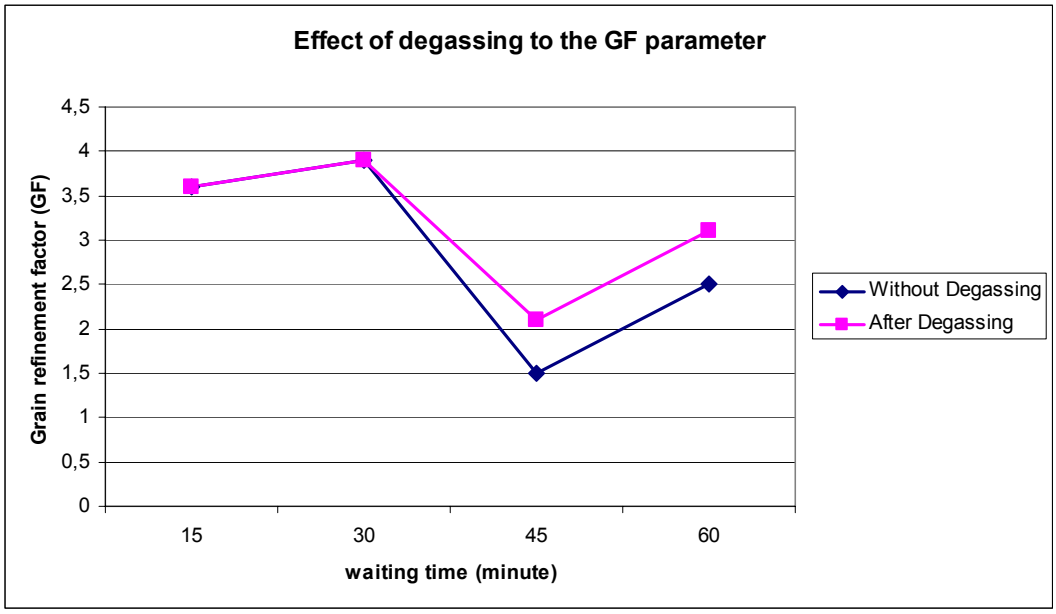

Figure 35. Effect of degassing to the GF parameter

4.2.5 Effect of Alloying Sequence to the thermal analysis results, microstructure and mechanical properties

To see the effect of master alloy addition sequence to the thermal analysis results, two procedures were used. In the first procedure firstly AlTi5B (grain refiner) was added and after 5 minutes Al10Sr (modifier) was added. In the second procedure opposite of the first procedure was done; first Al10Sr (modifier) was added and after 5 minutes AlTi5B (grain refiner) was added into the melt. And it was found that master alloy addition sequence has no effect on the thermal analysis parameters.

4.2.6 Interpretation of Thermal Analysis Results

4.2.6.1 Finding the Grain Refinement Factor Equation

To find the formula of the GF parameter of the Alu-Therm thermal analyzer the regression analysis was done. Before regression analysis the parameters that can be related to the grain size were determined, and these parameters are lowest temperature of the liquidus (Tll), time of the lowest temperature of the liquidus (Tll_{time}), highest temperature of the liquidus (Tlh), time of the highest temperature of the liquidus (Tlh_{time}) and the initial temperature at the thermal analysis cup (T_{inf}). The reason why these parameters were selected can be explained as: grain size is directly proportional to the depth of the undercooling and undercooling at the liquidus can be determined as the difference of the highest and lowest temperatures at the liquidus of the cooling curve and these points are Tll and Tlh. Grain size is also proportional to the length of the undercooling and approximate length of the undercooling can be calculated by the subtracting Tll_{time} from Tlh_{time} . These parameters are shown in Figure 36.

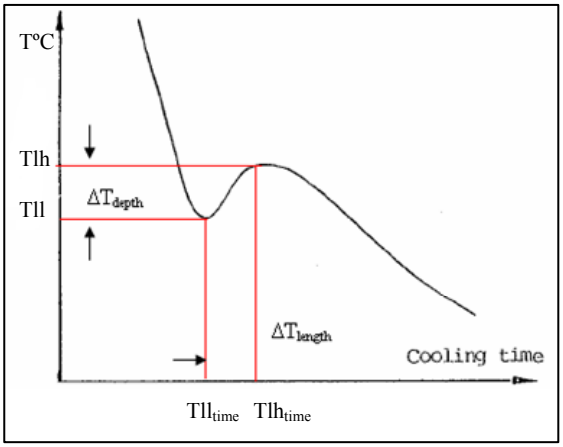

Figure 36. Schematic representation of Tll, Tlh, Tll_{time} and Tlh_{time} parameters

After finding the related parameters of the grain refinement factor (GF), regression analysis was done by using these parameters to find the formula of grain refinement factor (GF). The statistics of the regression analysis are given in Table 8.

Table 8. Regression analysis statistics of grain refinement factor

Regression Statistics	
Multiple R	0,95402653
R Square	0,91016662
Adjusted R Square	0,899958281
Standard Error	0,884555787
Observations	50

As it can be seen from Table 8, the results of the regression analysis is accurate because the R square value is equal to 0.91 which means that predicted grain refinement factors (GF) are 91% equal to original grain refinement factor which are calculated by the thermal analyzer. The comparison of the predicted and calculated GF values is given in Figure 37. The equation of the grain refinement factor predicted by regression analysis is the following:

$$GF = -\left(\frac{1}{Tll} * 457920.519\right) - \left(\frac{1}{Tll_{time}} * 480.676\right) + \left(\frac{1}{Tlh} * 375806.079\right) + \left(\frac{1}{Tlh_{time}} * 708.971\right) + \left(\frac{1}{T_{\inf}} * 10069.738\right) + 132.035 \quad (9)$$

From equation 9 it is understood that as the Tll increases and Tlh decreases, GF parameter increases which means that as the depth of the

undercooling (ΔT=Tlh-Tll) decrease, the grain size decreases. Also as the Tll_{time} increases and Tlh_{time} decreases, GF parameter of the thermal analyzer increases which means that as the length of the undercooling (ΔT_{length}= Tlh_{time}- Tll_{time}) decreases, the grain size decreases. These results are consistent with the results found in literature (Argyropoulos(1983)),(Charbonnier (1979)). Also the relationship between the pouring temperature and the grain size can be understood from the equation 9, which shows that as the pouring temperature increases grain size increases.

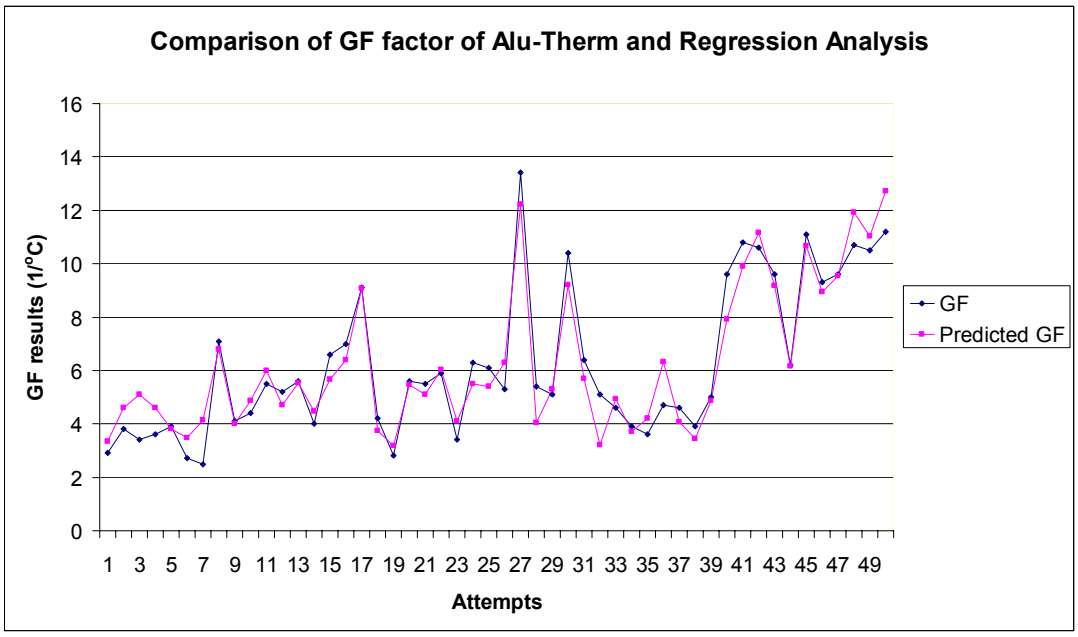

Figure 37. Comparison of GF factor of Alu-Therm and Regression Analysis

4.2.6.2 Finding the Relationship between Grain Refinement Factor and Dendrite Secondary Arm Spacing

After finding the relationship between grain refinement factor (GF) and grain size by comparison of the microstructures and GF values, thermal analysis and metallographic results were examined deeply. It was found that there is a direct relationship between GF parameter and dendrite secondary arm spacing and this relationship was proved by the regression analysis. The statistics of the regression analysis are given in Table 9.

Table 9. Regression analysis results of Dendrite secondary arm spacing

Regression Statistics	
Multiple R	0,881071914
R Square	0,776287718
Adjusted R Square	0,674600316
Standard Error	1,610093351
Observations	17

Table 9 shows that R square value of the regression analysis is 0.78 which means that predicted dendrite secondary arm spacing (DAS) calculated by regression analysis are 78 % same as the results measured by the image analyzer.

The equation of the dendrite arm spacing (DAS) calculated by regression analysis is as following:

$$DAS = \left(\frac{1}{Tll} * 284183.684\right) - \left(\frac{1}{Tll_{time}} * 595.618\right) - \left(\frac{1}{Tlh} * 390445.44\right) + \left(\frac{1}{Tlh_{time}} * 1206.14\right) - \left(\frac{1}{T_{\inf}} * 7213.073\right) + 206.620 \quad (10)$$

Since the relation between Tll ,Tlh, Tll_{time}, Tlh_{time} parameters and grain refinement factor (GF) values were found, same parameters (Tll ,Tlh, Tll_{time}, Tlh_{time}) were used in the regression analysis of dendrite arm spacing (DAS). The comparison of the measured and calculated dendrite arm spacing results are given in Figure 38.

The results of regression analysis show that dendrite secondary arm spacing of the alloy can be calculated just by using thermal analysis prior to casting. However these results are valid for the castings which have same cooling conditions, because grain size of the casting depends inversely on the cooling rate.

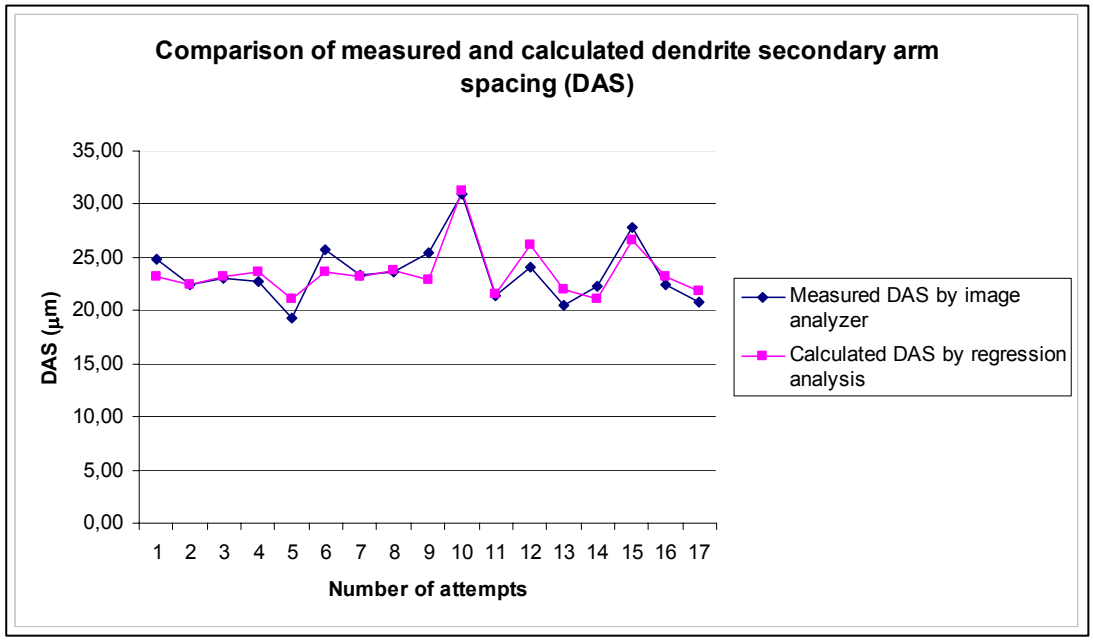

Figure 38. Comparison of measured and calculated dendrite secondary arm spacing (DAS)

4.2.6.3 Relationship between Tensile Strengths and Thermal Analysis results

It is known that tensile strength depends on the grain size and crack propagation points in the microstructure. Since grain size and crack propagation points are directly related to the grain refinement and modification, respectively; regression analysis was done by using thermal analysis parameters to find the relationship between these parameters and the tensile strength. The parameters that were used in regression analysis are: lowest temperature at the liquidus (Tll), time corresponding to lowest temperature of the liquidus (Tll_{time}), highest temperature of the liquidus (Tlh), time corresponding to highest temperature of the liquidus (Tlh_{time}) ,initial temperature at the thermal analysis cup (T_{inf}), lowest temperature of the solidus (Tsl), time corresponding to lowest temperature of the solidus

(Tsl_{time}), highest temperature of the solidus (Tsh), time corresponding to highest temperature of the solidus (Tsh_{time}).

The reasons why these parameters were selected:

- Tll and Tlh temperatures are related to depth of the undercooling at the liquidus, Tll_{time} and Tlh_{time} parameters are related to length of the undercooling at the liquidus and these parameters with T_{inf} determine the grain refinement factor.
- Tsl and Tsh temperatures are related to depth of the undercooling at the solidus. Tsl_{time} and Tsh_{time} parameters are related to length of the undercooling and these parameters determine the effectiveness of modification.

And statistics of the regression analysis is given in Table 10. These statistics show us that R square value is 0.78 which means that calculated (predicted) tensile strengths are 78% same as the results measured by tensile testing machine. Comparison of the measured and calculated tensile strength values is given in Figure 39.

Table 10. Regression analysis statistics of the tensile strength

Regression Statistics	
Multiple R	0,880712861
R Square	0,775655144
Adjusted R Square	0,70427269
Standard Error	14,3251655
Observations	30

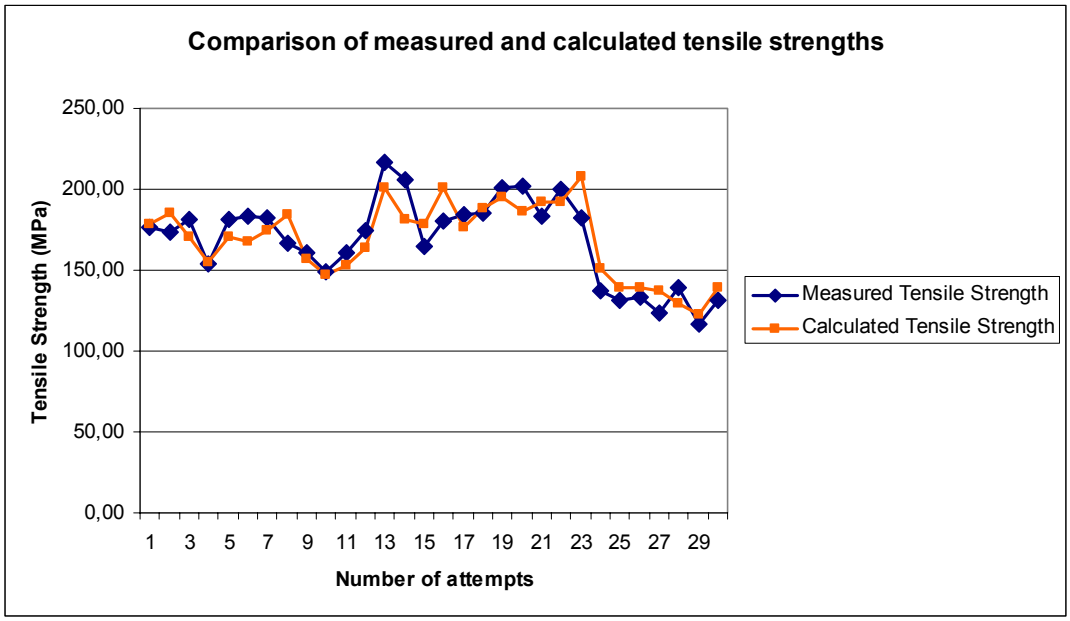

Figure 39. Comparison of measured and calculated tensile strengths

The equation of the tensile strength calculated by regression analysis is given as equation 11.

$$TensileStregth(MPa) = -(2.1730Tlh) + (1.959 * Tlh_{time}) + (9.106 * Tsl) - (0.455 * Tsl_{time}) - (2.281 * Tsh) + (0.293 * Tshtime) - (0.643 * T\inf) - 2107.349 \quad (11)$$

4.2.6.4 Relationship between Hardness and Thermal Analysis results

Since hardness is directly related to grain structure, the same thermal analysis parameters that were used to find the relationship between tensile strength and thermal analysis results were used to find the relationship between hardness and thermal analysis parameters. The statistics of the

regression analysis for hardness is given in Table 11. Comparison of measured and calculated brinell hardness values is given in Figure 40.

Table 11. Regression analysis statistics for hardness

Regression Statistics	
Multiple R	0,858372387
R Square	0,736803154
Adjusted R Square	0,624004506
Standard Error	2,364376417
Observations	31

Regression analysis statistics show that R square value is 0.73 which means that calculated (predicted) brinell hardness values are 73% same as the results measured by analog brinell hardness machine.

The equation of the brinell hardness found by regression analysis is as follows:

$$HB = -(3.263 * Tll) + (0.376 * Tll_{time}) + (4.256 * Tlh) - (0.212 * Tlht_{ime}) - (0.702 * Tsl) + (0.007 * Tsltime) + (0.643 * Tsh) - (0.066 * Tshtime) - (0.037 * T_{\inf}) - 454.545 \quad (12)$$

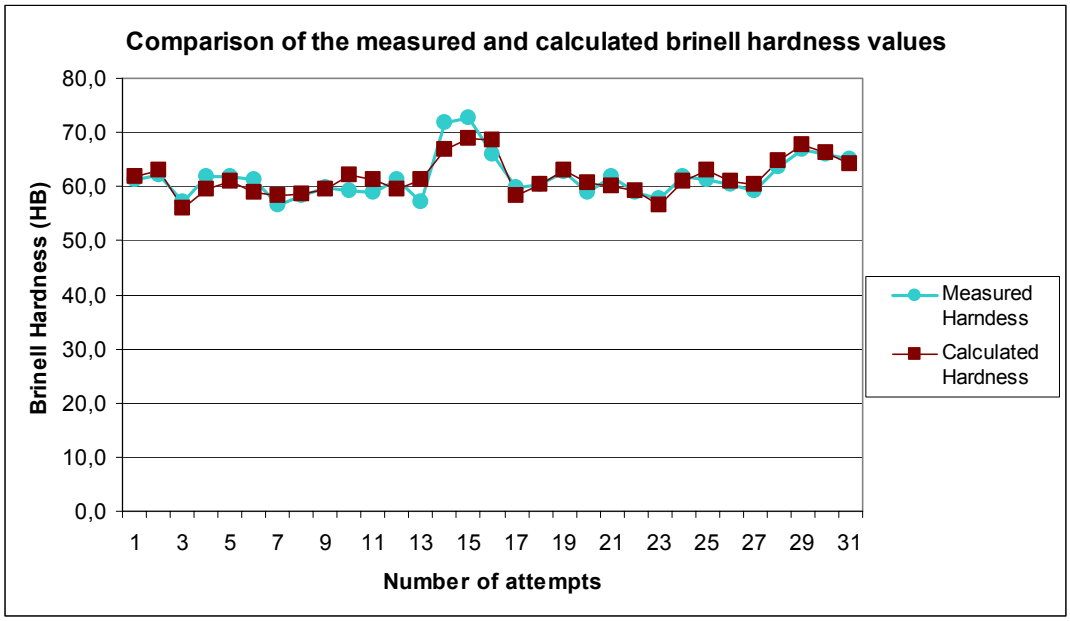

Figure 40. Comparison of the measured and calculate brinell hardness values

CHAPTER 5

CONCLUSION

A series of $AlSi_9Mg$ alloys with different amounts of grain refiner and modifiers were prepared and tested to reveal the effect of addition sequence and timing of grain refiner and eutectic modifier by using special aluminum thermal analyzer. The results obtained from thermal analyzer were compared with the metallographic and mechanical test results to find the relationship between these parameters. The findings showed that:

1. As the Ti content increases, the grain size of the alloy decreases and this relationship can be formulated in term of grain refinement parameter (GF) which can be obtained by linear regression analysis after the thermal analysis.
2. The time duration after the addition of grain refiner has a vital importance on the grain size because after 45 minutes waiting period fading begins and alloy grain size begins to increase. The grain refinement process can be understood from the cooling curve by interpretation of the time temperature cooling curve data.
3. As the amount of grain refiner increases in the melt the amount of undercooling and length of the undercooling at the liquidus begins to decrease.
4. The grain size of the casting is also found to be related to the pouring temperature. As the pouring temperature decreases, the grain size of the castings gets finer.

5. Regression analysis showed that grain refinement factor is inversely proportional to Tll, Tll_{time}, Tlh, Tlh_{time} and $T_{infusion}$ parameters of the thermal analysis.
6. The results show that the grain refinement factor (GF) is directly proportional to the dendrite secondary arm spacing of the alloy.
7. The regression analysis showed that dendrite secondary arm spacing can be predicted empirically prior to casting using thermal analysis determining Tll, Tll_{time}, Tlh, Tlh_{time} and $T_{infusion}$ temperatures on the cooling curves.
8. It is found that with strontium addition to the melt, there is a depression of the eutectic temperature and the depth of undercooling at the solidus increases.
9. The eutectic reaction is prolonged by strontium addition and by increasing the mass of the alloy sample poured in the test cup during thermal analysis.
10. Eutectic modification level could be found just from the difference between the eutectic temperature of the unmodified and modified alloy.
11. Regression analysis showed that the approximate tensile strength and brinell hardness of the alloy can be calculated prior to casting by thermal analysis by using Tll, Tll_{time}, Tlh, Tlh_{time}, $T_{infusion}$, Tsl, Tsl_{time}, Tsh and Tsh_{time} parameters of thermal analysis.
12. Derivative of the cooling curves calculated could be used to determine the phase transformation temperatures and the small changes in the undercooling at the liquidus and solidus temperatures.
13. Degassing by hexaflorethane after the addition of modification agent and grain refiner into the melt suppressed the effect of the modification agent and the melt responded as an unmodified alloy which resulted in failure of treatment. However thermal analysis and metallographic examination results proved that degassing by hexaflorethane had no effect on the grain refiner performance. For this reason either another method of degassing should be used or modification agent should be added after degassing by hexaflorethane.

14. Addition sequence of grain refiner and modification agent has no effect on the success of microstructure control. Which means that foundrymen can add grain refiner right before or after the modification.

REFERENCES

Aarflot A., (1985), “ Development of Melt Treatment”, Paper presented at the International Seminar on Refining and Alloying of Liquid Aluminum and Ferro Alloys (Trondheim, Norway).

Apelian D., Sigworth G.K., Whaler K.R., “Assessement of Grain Refinement and Modification of Al-Si Foundry Alloys by Thermal Analysis”, AFS Transactions, 92, p.297-307.

Argyropoulos S., Closset B., Gruzleski J.E. and Oger H., (1985),“ The Quantitative Control of Modification of Al-Si Foundry Alloys Using a Thermal Analysis Technique”, AFS Transactions, 91, p.351-357.

Arnberg L., Backerud L. and Klang H., (1982), "Met. Technol."

Backerud L. (1983) , "Light Met. Age", p.3-7

Backerud L., Gustafson P. and Klang H., (1991), "Aluminum", 67, 910

Banerji A. Reif W., (1987), " Solidification Processing (London: The Inst. Of Met.) " p.145

Banerji A., Reif W. and Feng Q., (1994) , "J. Mater. Sci." p.1958

Charbonnier J., Morice J., Portalier R., (1979), “Thermal Analysis of Aluminum Alloys to determine their suitability for casting”, AFS International Cast Metals Journal, p.39-44.
Cibula A. (1949), "J.Inst. Met." , 76, p.321

Clegg A.J., (1986), “ Aluminum degassing Pratice, Proceedings of the International Molten Aluminum Processing Conference, American Foundrymen’s Society”, p.369

Cook R., Cooper P.S., Kearns M.A., (1996), “TMS Light Metals”, 647

Crossley F.A. and Mondolfo L.F. (1951), "Trans AIME", 191, p.1143

Dahle A.K., Arnberg L., (1997), “Mater. Sci. Eng. “, 225,38

Davies I.G., Dennis J.M. and Hellawell A., (1970), " Metall. Trans." p.275

Davis J.R., (1994), "Aluminum and Aluminum Alloys", ASM Specialty Handbook, p.88

Easten Mark and St.John David, (1999), " Metall. Mater. Trans." , p.275

Fang Q.T., Anyalebechi P.N., O'Mahey R.J., and Granger D.A., (1987) " in Proceedings the Third International Solidification Conference (Sheffield, U.K.) ", Institute of Metals

Fine M.E. and Conley J.G., (1990), " Metall. Trans." A21, p.2609

Flemings M.C. and S.Metz, (1970) " AFS Transactions " Vol 78, p.453-460

Flemings Merton C. (1974a), "Solidification processing (eds) M. Stephen et al (USA: McGraw-Hill Inc.)" , ch.5, p.135

Flemings Merton C. (1974b), "Solidification processing (eds) M. Stephen et al (USA: McGraw-Hill Inc.)" , ch.5, p.151

Granger D. A. and Hammar L. D. , “Grain Size Control in EC Aluminium ,” Proceedings of 3rd International Conference on Aluminium Alloys, Vol. 1,Trondheim, Norway, 22-26 June 1992, 9-14, Publ. SINTEF .

Greer A.L., Bunn A.M., Tronche A., Evans P.V., Bristow D.J., (2000)“Acta Mater.” , vol.48, p.2823

Gruzleski John E., Closset Bernard M., (1999) "The Treatment of Liquid Aluminum-Silicon Alloys", The American Foundrymen's Society, Inc. , p.13-14

Guzowski M.M., Sigworth G.K. and Sentner D.A., (1987), "Metall. Trans.", A18, p.603

Honma U. and Oya S., (1983) , "Aluminum" ,Vol. 59, p.E169,172

http://www.key-to-metals.com

Jiang H., Sokolowski J.H., Djurdjevic M.B.,Evans W.J,(1990), “Recent advances in automated evaluation and on-line prediction of Al-Si eutectic modification level”, AFS Transactions 505-510.

Johnsson M and Backerud L., (1996), "Z.Metallkd.", 87, 216.

Johnsson M. (1993), " Light Metals (ed.) S.K. Das (Warrendale, PA:TMS)", p. 769

Johnsson M., Backerud L., (1992) , “Nucleus in grain refined Al after addition of Ti- and B containing master alloys”, Z. Metallkd. 83 (11) p.774–780.

Jones G.P. , (1988), "in Proc. Conf. solidification processing (eds.) J. Bleech and H. Jones (London: The Institute of Metals", p.496

Jones G.P. and Pearson J., (1976), "Metall. Trans." , B7, p.223

Kearns M.A., Thistlethwaite S.R., Cooper P.S., (1996), “TMS Light Metals”, 713

Kissling R.J. and Wallace J.F., (1963), “Gas Porosity in Aluminum Casting”, Penton publishing.

Kiusalaas R., (1986), " Relation Between Phases Present in Master Alloys of the Al-Ti-B Type", Thesis, University of Stockholm.

Kurz W. and Fisher D.J., (1984), " Fundamentals of solidification (Switzerland: Trans. Tech. Publications" , p.47

Lebahn D.L., (1982), “Effects Observed When Fluxing Aluminum with Mixed Gases”, Paper presented at the Pacific Northwest Conference on Advances in Aluminum Casting, Spokane, WA.

Limmaneevichitr C. and Eidhed W. (2002), “Fading mechanism of grain refinement of aluminum–silicon alloy with Al–Ti–B grain refiners”, Materials Science and Engineering A, 2003, 349: pp. 197-206.

Marcantonio J.A. and Mondolfo L.F., (1971), "Metall. Trans.", p.465

Maxwell I. and Hellawell A., (1972), "Metall Trans.", p.1487

McCartney D.G. (1989), " Int. Mater. Rev. " p.247

Mohanty P.S. and Gruzleski J.E. , (1995), "Acta Metall. Mater." P.43
Mohanty P.S., Samuel F.H. and Gruzleski J.E. (1995), " Metall. Mater. Trans. " B.26 p.103

Molland R.F., Dorne J.E. and Davidson N., (1979),“A Low Emission Process for the Melt Treatment of Aluminum Alloys”, Paper presented at U.S.EPA Conference on Control of Particulate Emissions in Primary Nonferrous Metals Industries (Monterey, CA), Environmental Protection Agency.

Mondolfo L.F, Farooq S, (1987), " in Proceedings of the Third International Solidification Conference (Sheffield, U.K.) ", Institute of Metals p.133

Nafisi S., Ghomashchi R., Hedjazi J., Boutorabi S.M.A., (2004), “New Approaches to Melt Treatment of Al-Si Alloys: Application of Thermal Analysis Technique”, AFS Transactions 2004, p.167-177.

Nagel G. and Portalier R., (1980) , " AFS Int. Cast Met. Journal" , Vol.5, p. 2

Oya S., Fujii T., Ortaki M.,(1984) " Jpn. Inst. Light Met." Vol 34, p.511 – 516

Rapp R.A. and Zheng X., (1991), "Metall Trans.", A22 3071

Schumacher P. and Greer A.L. (1994a), " Mater. Sci. Eng." ,A178, 309.

Schumacher P. and Greer A.L. (1994b), " Mater. Sci. Eng." ,A181, 1335.

Sigworth G.K. and Guzowsky M.M., (1985) " Trans. AFS " , Vol 93, p.907 – 912

Sigworth G.K., (1984) , "Metall.Trans." , A15, 277
Sigworth G.K., (1986) , "Metall.Trans." , A22, 349

Sigworth G.K., (1986), "in International Molten Aluminum Processing Conference", The American Foundrymen's Society, Inc. , p.75-89

Snow G., Patthe D. and Walker G., (1987), “An Efficient degassing System for the Aluminum Casthouse, Light Metals. The Metallurgical Society”, p.717

Sokolowski J.H., Djurdjevic M.B., Kierkus C.A., Northwood D.O., (2001), “J. Mater. Process. Technol.”, 109,174.

Spittle J.A., Sadli S.B., (1995), “Mater. Sci. Technol.” 11, 533

St.John D.H., (1990), " Acta Metall. Mater." 38, 631

Tenekedjiev Ned, Mulazimoglu Hasim, Closset Bernard, Gruzleski John, (1995), “Microstructure and Thermal Analysis of Strontium-Treated Aluminum-Silicon Alloys”, p.1-62

Vader M. and Noordegraaf J., (1989), "Light Metals (ed.) P.G. Campbell (Warrendale, PA:TMS)" , p.937

Volmer M and Weber A. , (1925), "Z.Krift. Phys. Chem." 119, 277.

Wang T.H., Guo M.H., Chen S.L., Liao C.L., (1998), “TMS Light Materials” , 969.

Whitehead A.J. and Danilak S.A., (1997), “The Development of a commercial Al-3%Ti-0,15%C Grain Refining Master Alloy”,The 126th TMS Annual Meeting & Exhibtion, February 9-13th, 1997, Orlando, Florida, USA.

Table A.1. Thermal analysis results and corresponding metallographic and mechanical results

Alloy Name	Waiting Time (min)	GF	M(574,1) (°C)	Tref (°C)	TII (°C)	TII time (sec)	TIh (°C)	TIh time (sec)	Tsl (°C)	Tsl time (sec)	TE=Tsh (°C)	Tsh time (sec)	dTS (°C)	Tinfusion (°C)	TL ΔT length (sec)	TL ΔT (°C)	Ts length (sec)	Tensile Strength (Mpa)	Elongation (%)	Hardness HB
Alloy I	15 min	2,7	-0,7	574,1	577,8	56,3	580,0	65,8	578,5	94,7	574,8	105,5	2,0	820,6	9,5	2,2	10,8	176,02	2,76	61,3
	30 min	2,9	1,0	574,1	577,4	54,2	579,3	65,0	570,9	112,4	573,1	165,7	2,2	738,5	10,8	1,9	53,3	135,48	2,24	62,1
	45 min	3,8	1,3	574,1	577,0	44,3	578,0	55,1	571,0	101,5	572,8	190,4	1,8	718,9	10,8	1,0	88,9	173,79	4,12	57,0
	60 min	3,4	0,2	574,1	576,9	40,5	578,1	49,3	572,4	90,8	573,9	143,9	1,5	706,6	8,8	1,2	53,1	160,19	2,90	62,0
Alloy II	15 min	3,6	3,7	574,1	581,4	65,1	582,9	74,0	569,1	157,1	570,4	267,5	1,3	759,1	8,9	1,5	110,4	181,56	-	65,8
	30 min	3,9	3,4	574,1	581,6	66,0	583,4	77,8	568,8	161,5	570,7	267,2	1,9	767,8	11,8	1,8	105,7	152,97	-	61,7
	45min	1,5	3,3	574,1	581,2	84,8	582,7	95,6	570,8	283,0	570,8	295,8	0,0	797,4	10,8	1,5	12,8	154,36	3,28	61,2
	60 min	2,5	2,7	574,1	581,0	69,0	582,4	79,9	568,7	161,6	571,4	287,8	2,8	769,7	10,9	1,4	126,2	137,15	1,06	56,6
Alloy III	15 min	7,1	3,4	574,1	583,1	51,2	584,0	59,1	569,7	144,9	570,7	256,3	1,0	721,4	7,9	0,9	111,4	181,56	-	58,3
	30 min	4,1	3,3	574,1	581,8	90,8	582,7	100,7	568,6	198,7	570,8	281,8	2,2	814,4	9,9	0,9	83,1	183,23	5,11	59,8
	45 min	4,4	2,0	574,1	582,8	75,9	583,8	85,8	570,0	181,5	572,1	277,1	2,1	779,7	9,9	1,0	95,6	182,68	-	53,0
	60 min	5,5	1,6	574,1	582,4	49,3	583,2	60,1	570,3	122,3	572,5	176,5	2,2	729,9	10,8	0,8	54,2	217,10	9,35	59,3
Alloy IV	15 min	5,2	2,6	574,1	583,5	67,1	584,8	77,0	569,5	159,7	571,5	254,3	2,1	788,6	9,9	1,3	94,6	186,01	4,70	59,0
	30 min	5,5	1,9	574,1	584,0	61,1	585,5	88,0	570,0	146,0	572,2	240,7	2,2	774,8	26,9	1,5	94,7	166,57	4,12	61,2
	45min	5,6	1,8	574,1	583,9	64,0	584,9	72,9	570,4	154,8	572,3	243,6	1,9	773,9	8,9	1,0	88,8	160,47	1,74	57,1
	60 min	4	2,0	574,1	582,7	69,9	583,9	79,8	569,7	154,6	572,1	240,4	2,4	794,9	9,9	1,2	85,8	180,45	3,51	54,6
Alloy V	15 min	6,6	0,0	574,1	584,2	42,3	586,1	50,2	572,3	103,4	574,1	181,3	1,8	744,3	7,9	1,9	77,9	149,15	2,70	71,9
	30 min	7	-0,8	574,1	584,1	42,5	585,8	49,4	573,8	102,6	574,9	135,1	1,1	731,7	6,9	1,7	32,5	161,16	2,95	72,8
	45 min	9,1	-1,5	574,1	584,9	17,7	585,7	23,6	575,2	62,2	575,6	72,1	0,4	652,6	5,9	0,8	9,9	174,5	2,70	65,8
	60 min	4,2	-0,7	574,1	581,3	46,3	584,2	54,2	574,3	104,8	574,8	128,6	0,5	746,5	7,9	2,9	23,8	-	-	62,7
Alloy VI	15 min	5,6	2,3	574,1	580,2	69,9	581,2	77,8	569,4	169,5	571,8	284,0	2,4	728,4	7,9	1,0	114,5	216,93	4,55	59,8
	30 min	5,5	2,9	574,1	579,8	53,1	581,2	61,0	568,6	131,1	571,2	225,9	2,6	735,1	7,9	1,4	94,8	198,51	3,00	60,4
	45min	5,9	-1,8	574,1	581,2	42,3	582,5	50,2	575,6	105,4	575,9	136,0	0,3	721,5	7,9	1,3	30,6	205,98	3,40	60,4
	60 min	3,4	-1,5	574,1	580,1	54,2	581,7	64,0	575,3	121,3	575,6	152,9	0,3	763,6	9,8	1,6	31,6	165,16	2,90	62,7
Alloy VII	15 min	6,1	-1,5	574,1	580,3	51,2	581,4	60,1	575,0	114,3	575,6	171,5	0,6	736,4	8,9	1,1	57,2	164,36	2,20	59,0
	30 min	5,3	-1,6	574,1	580,2	43,4	580,9	53,3	575,6	117,4	575,7	147,0	0,1	701,8	9,9	0,7	29,6	180,1	3,00	61,9
	45 min	13,4	-1,2	574,1	580,4	33,4	580,4	33,4	575,1	108,4	575,3	138,1	0,2	678,8	0,0	0,0	29,7	184,64	1,60	59,0
	60 min	5,4	0,6	574,1	577,3	20,7	577,8	31,5	573,3	84,8	573,5	112,3	0,1	648,9	10,8	0,5	27,5	185,7	3,50	57,6
Alloy VIII	15 min	10,4	-0,9	574,1	581,5	36,1	581,7	41,3	575,0	127,5	575,0	127,5	0,0	682,1	5,2	0,2	0,0	195,31	5,50	61,9
	30 min	7,3	-0,6	574,1	577,0	43,3	579,4	58,1	574,7	152,9	574,7	152,9	0,0	699,0	14,8	2,4	0,0	200,64	3,90	61,2
	45min	7,6	-1,3	574,1	577,2	41,3	579,5	59,1	575,4	150,9	575,4	150,9	0,0	723,8	17,8	2,3	0,0	201,71	3,60	60,4
	60 min	7,7	-1,7	574,1	577,2	36,6	579,5	53,4	575,8	172,8	575,8	172,8	0,0	690,9	16,8	2,3	0,0	-	-	59,1
Alloy IX	15 min	6,4	0,8	574,1	582,0	39,3	583,9	47,2	571,6	107,4	573,3	185,5	1,7	716,2	7,9	1,9	78,1	215,59	5,30	63,6
	30 min	2,8	-0,2	574,1	581,2	75,9	583,5	85,9	572,8	166,9	574,3	215,2	1,5	768,9	10,0	2,3	48,3	183,57	2,30	66,7
	45min	4,6	-1,4	574,1	580,9	40,5	583,1	49,3	575,2	96,7	575,5	152,9	0,3	709,6	8,8	2,2	56,2	200,11	4,50	66,1
	60 min	3,9	-0,4	574,1	579,9	73,5	581,5	85,1	574,1	155,4	574,5	184,4	0,4	759,3	11,6	1,6	29	182,5	2,10	65,0